A&A 476, 893–909 (2007)
DOI: 10.1051/0004-6361:20078132

Astronomy & Astrophysics

Evolution of massive AGB stars

II. model properties at non-solar metallicity and the fate of Super-AGB stars⋆

L. Siess⋆⋆

Institut d'Astronomie et d'Astrophysique, Université Libre de Bruxelles, CP 226, 1050 Brussels, Belgium
e-mail: siess@astro.ulb.ac.be

Received 21 June 2007 / Accepted 18 September 2007

ABSTRACT

Context. Massive AGB (hereafter super-AGB or SAGB) stars ignite carbon off-center and have initial masses ranging between $M_{\rm up}$, the minimum initial mass for carbon ignition, and $M_{\rm mas}$ the minimum mass for the formation of an iron core collapse supernova. In this mass interval, stars more massive than $M_{\rm n}$ will undergo an electron capture supernova (EC-SN).
Aims. We study the fate and selected evolutionary properties of SAGB stars up to the end of the carbon burning phase as a function of metallicity and core overshooting.
Methods. The method is based on the analysis of a large set of stellar models covering the mass range 5−13 $M_{\odot}$ and calculated for 7 different metallicities between $Z = 10^{-5}$ and twice solar. Core overshooting was considered in two subsets for $Z = 10^{-4}$ and 0.02. The models are available online at http://www-astro.ulb.ac.be/~siess/database.html. The fate of SAGB stars is investigated through a parametric model which allows us to assess the role of mass loss and of the third dredge-up.
Results. Our main results can be summarized as follows: a) prior to C-burning, the evolution of SAGB stars is very similar to that of intermediate-mass stars, being more luminous, b) SAGB stars suffer a large He enrichment at the end of the second dredge-up, c) the limiting masses $M_{\rm up}$, $M_{\rm n}$ and $M_{\rm mas}$ present a nonlinear behavior with Z, characterized by a minimum around $Z = 10^{-4}$, d) the values of $M_{\rm up}$, $M_{\rm n}$ and $M_{\rm mas}$ are decreased by ∼2 $M_{\odot}$ when core overshooting is considered, e) our models predict a minimum oxygen-neon white dwarf mass of ∼1.05 $M_{\odot}$, f) the determination of $M_{\rm n}$ is highly dependent on the mass loss and core growth rates, g) the evolutionary channel for EC-SN is limited to a very narrow mass range of $\lesssim$1−1.5 $M_{\odot}$ width and this mass window can be further decreased if some metallicity scaling factor is applied to the mass loss rate, h) the final fate of SAGB stars is connected to the second dredge-up and this property allowed us to refine the initial mass range for the formation of EC-SN. We find that if the ratio of the mass loss rate to the core growth rate averaged over the post carbon-burning evolution $\zeta = \left|\overline{\dot{M}}_{\rm loss}/\overline{\dot{M}}_{\rm core}\right|$ is greater than about 70−90, the evolutionary path to EC-SN is not accessible.

Key words. stars: evolution – stars: AGB and post-AGB – stars: supernovae: general – stars: white dwarfs – stars: mass-loss

1. Introduction

Stars can be divided into different mass categories depending on their evolution and the nature of their stellar remnant. This differentiation is the result of some common physical properties shared by the stellar matter (e.g. Maeder & Meynet 1989; Chiosi et al. 1992). The minimum mass for carbon ignition is traditionally referred to as $M_{\rm up}$ (e.g. Becker & Iben 1979, 1980) and $M_{\rm mas}$ represents the mass limit above which the star ignites neon at the center and evolves throughout all the nuclear burning stages, leading to iron core collapse supernova (e.g. Woosley et al. 2002). Objects we refer to as super-AGB (SAGB) stars have initial masses between $M_{\rm up}$ and $M_{\rm mas}$. Their evolution is characterized by the off-center ignition of carbon in conditions of partial degeneracy followed by the inward propagation of a carbon deflagration that transforms the CO core into a oxygen-neon (ONe) mixture (Garcia-Berro & Iben 1994; Siess 2006a, hereafter Paper I). When the flame reaches the center, C-burning proceeds temporarily outward in a shell before complete extinction. At this time, the internal stellar structure is very similar to that of lower mass AGB stars, except that their cores are more massive and essentially made of neon and oxygen. SAGB stars can thus be considered as the high-mass counterpart of AGB stars and, as such, they will subsequently suffer recurrent thermal instabilities in the He-burning shell (HeBS).

If after the carbon burning phase the degenerate core mass grows to the critical value of $M_{\rm EC} \sim 1.37\ M_{\odot}$ (Nomoto 1984), electron-capture reactions are activated at the center and induce core collapse, leading to the formation of a neutron star (Miyaji et al. 1980). Whether or not the SAGB core mass reaches this critical value depends on the interplay between mass loss and core growth which are complicated functions of the initial conditions (mass, composition, stellar rotation, extra-mixing, etc.). If during the post-C burning evolution the mass loss rate is high enough, the envelope is lost before the core mass reaches $M_{\rm EC}$ and the remnant is a ONe white dwarf (WD). On the contrary, if the mass loss rate is not large enough, the endpoint of SAGB evolution is the formation of a neutron star. The initial stellar mass that separates these two regimes is referred to as $M_{\rm n}$ and represents the minimum initial mass for the formation of a neutron star.

The first studies of SAGB stars focused on the explosive stages following the activation of electron capture reactions in the ONe core (Miyaji et al. 1980; Nomoto 1981; 1984; Hillebrandt et al. 1984; Miyaji & Nomoto 1987;

⋆ Tables 4 and 5 are only available in electronic form at http://www.aanda.org
⋆⋆ FNRS research associate.

Gutiérrez et al. 1996) and as shown by the recent literature on the subject (Wanajo et al. 2003; Dessart et al. 2003; Kitaura et al. 2006) this field is still currently under active investigation. The basis of the (non explosive) evolution of SAGB stars was laid down in the 90's in a series of papers by García-Berro & Iben (1994), Ritossa et al. (1996), García-Berro et al. (1997), Iben et al. (1997) and Ritossa et al. (1999). Recently, new models have been computed for solar (Gil-Pons & García-Berro 2002; Siess 2006a; Doherty & Lattanzio 2006; Poelarends et al. 2006) and primordial composition (Gil-Pons et al. 2005, 2007) showing a renewal of interest for this specific stellar population.

Although the evolutionary properties of SAGB stars are globally well established, open questions and large uncertainties still remain. As an illustration, the relation between the initial mass and the final fate of SAGB stars has not received much attention (Poelarends et al. 2007). The fraction of stars with initial mass between $M_{\rm up}$ and $M_{\rm mas}$ which evolve into the ONe WD and electron capture supernova (EC-SN) channels is largely uncertain and very dependent on composition, mass loss rate or internal mixing (Eldridge & Tout 2004). In addition, little is known about the nucleosynthesis of s-nuclei during the thermally pulsing super-AGB (TP-SAGB) phase (Ritossa et al. 1996) and about the possibility (Sumiyoshi et al. 2001; Wanajo et al. 2003) or not (Kitaura et al. 2006) of r-process nucleosynthesis during the EC-SN explosion. The lack of realistic models covering a large range of metallicities means the contribution of SAGB stars to galactic chemical evolution is rather speculative.

In this paper we address some of the above mentioned issues using two homogeneous sets (with and without core overshooting) of SAGB models which cover a wide range of initial masses and compositions. In particular, emphasis is placed upon the dependence of $M_{\rm up}$ and $M_{\rm mas}$ on the initial composition, treatment of core overshooting and interplay between mass loss and core growth.

Observational evidence of SAGB stars has been indirectly provided by the study of neon novae (José & Hernanz 1998) which are characterized by a neon overabundance and the presence of Si-Ca nuclei in their ejecta (José et al. 2001). Recently Gil-Pons et al. (2003) showed that approximately 1/3 of the observed novae outbursts may host an ONe WD. They are thus quite numerous and this may explain in part why the mass distribution of WDs in galactic novae systems exhibits a peak around 1 $M_\odot$ (Webbink 1990).

Concerning single WDs, their mass distribution presents the canonical peak value around 0.6 $M_\odot$ but also displays an extended tail toward higher masses characterized by an excess with masses between ∼1.0 and 1.2 $M_\odot$ (Finley et al. 1997; Marsh et al. 1997; Vennes 1999; Liebert et al. 2005). The origin of these massive WDs is not clearly established and different options have been proposed (Weidemann 2000). They rely on the merging of CO WDs as a result of binary evolution (e.g. Segretain et al. 1997; Guerrero et al. 2004), on the lifting effect of rotation that is able to increase the WD mass significantly by the time the first thermal pulse develops (Dominguez et al. 1996) or on the evolution of stars more massive than $M_{\rm up}$, i.e. on SAGB stars (e.g. Iben et al. 1997). In any case, without knowledge of the mass, identification of isolated ONe WDs is extremely difficult because their cores are covered by a C/O layer coming from the accretion of the ashes of shell He burning, surrounded by a H and He rich envelope which makes them spectroscopically almost indiscernible from C/O WDs.

Recent identification of the progenitors of type II-P SNe revealed that these explosions tend to be associated with red supergiants with masses lower than about 15 $M_\odot$. Of particular interest in our case are the mass estimates for SN2003gr (6−12 $M_\odot$, Hendry et al. 2005), SN2004A (7−12 $M_\odot$, Hendry et al. 2006), SN2005cs (7−13 $M_\odot$, Maund et al. 2005) and SN2006my (7−15 $M_\odot$, Li et al. 2007). The robust limits set on the mass of these progenitors rule out the possibility of a scenario involving the explosion of massive stars surrounded by a thick ($\gtrsim$15 $M_\odot$) hydrogen envelope (Zampieri et al. 2003). Instead it favors the alternative model developed by Chugai & Utrobin (2000) of a low-energy explosion involving a low-mass star, potentially a SAGB star, as was originally proposed for the Crab Nebula (Hillebrandt 1982; Nomoto et al. 1983). SAGB stars thus appear to play a central role in type II-P SNe and further investigations into their ultimate evolution is of prime interest.

The transition masses are fundamental quantities not only in the framework of improving our knowledge of the evolution of massive AGB stars and testing our models, but also in relation to many astrophysical fields. A better determination of $M_{\rm up}$ and $M_{\rm n}$ will provide useful information concerning the initial-final mass relation of very massive (>1 $M_\odot$) WDs (see Ferrario et al. 2005 for an interesting discussion of the implication of a high mass tail in the WD mass distribution in terms of binary mergers) which is a fundamental ingredient for modeling WD populations, or to estimate the amount of mass returned to the interstellar medium. Changing the values of $M_{\rm n}$ and $M_{\rm mas}$ modifies the rate of iron core collapse SN (type II, Ib and Ic) which indirectly influences the composition, kinematics and structure of the interstellar medium (e.g. Ratnatunga & Van Den Bergh 1989) and thus the process of star formation (e.g. Cappellaro et al. 2005). Furthermore, the stellar yields are directly related to these limiting masses because depending on the evolutionary endpoint, the nucleosynthetic output will be different. In this respect, the yields from SAGB stars remain largely unknown.

The plan of this paper is as follows: in the next section we present the modifications made to our stellar evolution code with respect to Siess (Paper I) and the initial compositions used for our models. In Sect. 3, we provide a general description of the evolutionary features of SAGB stars up to the beginning of the TP-SAGB phase as a function of metallicity, focusing on the carbon burning phase. Then we analyze the different mass transitions, $M_{\rm up}$ and $M_{\rm mas}$, and in Sect. 4.3, with the help of a simple model, we investigate the dependence of $M_{\rm n}$ on mass loss and core growth rates. In Sect. 5 we analyze the fundamental role of the second dredge-up and discuss the implications of these transition masses in terms of He core properties. Finally, in Sect. 7, we summarize our results.

2. Input physics and initial models

Our models are calculated with the stellar evolution code STAREVOL as described in Paper I with the following differences concerning the mass loss rate, the treatment of convective mixing and the initial composition.

For the mass loss, we use Reimers formula (1975) with $\eta = 1$ and a correction factor $\sqrt{Z/Z_\odot}$ (Kudritzki et al. 1987) until the end of the core helium burning and then switch to the Vassiliadis & Wood (1993) prescription without metallicity dependence. It should be noted that little mass is removed by the end of He burning ($M_{\rm HeBS}$ in Table 1) and in the most conservative case where this scaling is not applied to the Reimers law, we find that at most an additional ∼0.1 $M_\odot$ is lost. This represents less than ∼1−2% of the stellar mass. So, as a conclusion, our computations are almost equivalent to ignoring this correction factor.

Table 1. Selected evolutionary properties prior to carbon ignition including the dredge-up features. The quantities shown are: main sequence lifetime ($\tau_{\rm H}$ in 10^6 yr), maximum extent of the convective H-burning core ($m^{\rm H}_{\rm conv}$ in $M_\odot$), time of completion of the 1DUP ($t_{\rm 1DUP}$ in 10^6 yr) and mass coordinate of the convective envelope at this moment ($m_{\rm 1DUP}$ in $M_\odot$), stellar mass at core He ignition ($M_{\rm He}$ in $M_\odot$), duration of the core He burning phase ($\tau_{\rm He}$ in 10^6 yr), maximum extent of the convective He-burning core ($m^{\rm He}_{\rm conv}$ in $M_\odot$), stellar mass at central He exhaustion ($M_{\rm HeBS}$ in $M_\odot$), central ^{12}C and ^{16}O mass fractions at He exhaustion, time ($t_{\rm 2DUP}$ in 10^6 yr) when the convective envelope reaches its deepest extent ($m_{\rm 2DUP}$ in $M_\odot$) after central He burning, central ^{16}O and ^{20}Ne at the end of C-burning.

$M_{\rm ini}$	$\tau_{\rm H}$	$m^{\rm H}_{\rm conv}$	$t_{\rm 1DUP}$	$m_{\rm 1DUP}$	$M_{\rm He}$	$\tau_{\rm He}$	$m^{\rm He}_{\rm conv}$	$M_{\rm HeBS}$	^{12}C	^{16}O	$t_{\rm 2DUP}$	$m_{\rm 2DUP}$	^{16}O	^{20}Ne
							$Z = 0.00001$							
7.0	34.766	2.225	41.516	1.782	6.999	5.966	0.673	6.999	0.360	0.640	41.967	1.012	0.640	0.000
7.5	30.819	2.448	36.632	1.930	7.499	5.201	0.766	7.498	0.327	0.673	36.964	1.060	0.673	0.000
7.7	30.251	2.530	35.469	1.967	7.699	4.662	0.761	7.698	0.348	0.652	35.805	1.066	0.568	0.311
8.0	27.613	2.668	32.630	2.084	7.999	4.536	0.855	7.998	0.319	0.681	32.902	1.131	0.594	0.299
8.5	24.962	2.875	29.269	2.219	8.499	3.912	0.910	8.498	0.331	0.669	29.510	1.185	0.588	0.306
9.0	22.749	3.110	26.560	2.386	8.999	3.490	1.013	8.998	0.317	0.683	26.744	1.258	0.597	0.307
9.5	20.865	3.345	24.288	2.546	9.499	3.164	1.127	9.498	0.283	0.717	24.429	2.696	0.641	0.274
10.0	19.284	3.575	22.384	2.666	9.999	2.877	1.205	9.998	0.272	0.728	22.510	2.890	0.656	0.261
10.5	17.904	3.816	20.754	2.835	10.499	2.659	1.344	10.498	0.232	0.768	20.851	3.133	0.702	0.231
11.0	16.711	4.078	19.286	3.006	10.999	2.408	1.446	10.998	0.225	0.775	19.370	3.321	0.713	0.219
11.5	16.240	4.294	18.551	3.130	11.499	2.166	1.522	11.498	0.211	0.789	18.628	3.507	0.729	0.207
12.0	14.742	4.595	16.938	3.284	11.999	2.072	1.624	11.998	0.244	0.756	17.008	3.697	0.687	0.242
							$Z = 0.0001$							
7.0	35.499	2.284	42.561	1.828	6.999	6.218	0.711	6.997	0.322	0.678	42.954	1.021	0.678	0.000
7.2	34.809	2.383	41.140	1.863	7.199	5.566	0.714	7.197	0.341	0.659	41.537	1.029	0.659	0.000
7.5	31.388	2.494	37.322	1.973	7.499	5.287	0.785	7.497	0.333	0.667	37.634	1.067	0.621	0.169
8.0	28.061	2.706	33.228	2.129	7.999	4.673	0.883	7.997	0.281	0.719	33.477	1.142	0.640	0.259
8.5	25.326	2.920	29.744	2.278	8.499	4.024	0.945	8.497	0.321	0.679	29.958	1.196	0.590	0.310
9.0	23.048	3.145	26.912	2.430	8.999	3.532	1.023	8.997	0.325	0.674	27.092	1.277	0.588	0.311
9.5	21.130	3.383	24.613	2.583	9.498	3.201	1.133	9.497	0.300	0.700	24.756	2.683	0.623	0.285
10.0	19.502	3.615	22.626	2.752	9.998	2.892	1.230	9.996	0.299	0.701	22.748	2.893	0.629	0.278
10.5	18.852	3.865	21.734	2.899	10.498	2.673	1.367	10.496	0.244	0.756	21.827	3.071	0.692	0.233
11.0	17.600	4.107	20.104	3.082	10.998	2.324	1.460	10.996	0.278	0.722	20.190	3.261	0.654	0.259
11.5	16.496	4.367	18.884	3.237	11.498	2.225	1.573	11.496	0.258	0.742	18.956	3.461	0.676	0.245
12.0	14.874	4.634	17.167	3.342	11.998	2.156	1.624	11.996	0.263	0.736	17.240	3.655	0.670	0.249
							$Z = 0.001$							
7.5	32.104	2.377	38.606	1.953	7.495	5.790	0.764	7.485	0.340	0.659	38.935	1.053	0.659	0.000
7.7	30.630	2.460	36.632	2.005	7.695	5.354	0.771	7.685	0.364	0.634	36.955	1.066	0.551	0.320
8.0	28.637	2.611	34.262	2.115	7.995	5.068	0.864	7.984	0.304	0.695	34.520	1.129	0.612	0.281
8.5	26.841	2.793	31.518	2.247	8.495	4.234	0.931	8.484	0.313	0.686	31.742	1.185	0.604	0.294
9.0	23.440	3.020	27.641	2.428	8.995	3.830	1.023	8.983	0.317	0.682	27.816	1.256	0.597	0.305
9.5	21.449	3.245	25.179	2.573	9.494	3.418	1.117	9.483	0.300	0.699	25.323	2.638	0.620	0.288
10.0	20.636	3.482	23.804	2.727	9.994	2.906	1.198	9.983	0.317	0.682	23.932	2.824	0.606	0.296
10.5	18.318	3.712	21.389	2.915	10.494	2.844	1.344	10.482	0.246	0.752	21.482	3.095	0.684	0.242
11.0	17.067	3.961	19.876	3.030	10.993	2.615	1.409	10.982	0.254	0.745	19.963	3.248	0.676	0.248
11.5	15.971	4.199	18.536	3.217	11.493	2.393	1.529	11.481	0.267	0.731	18.610	3.480	0.660	0.260
12.0	15.729	4.453	17.975	3.355	11.992	2.097	1.615	11.980	0.290	0.708	18.045	3.613	0.639	0.270
							$Z = 0.004$							
8.1	28.586	2.515	29.216	1.164	8.089	5.524	0.783	8.023	0.335	0.659	34.983	1.063	0.581	0.297
8.3	27.365	2.585	27.940	1.200	8.289	5.287	0.834	8.219	0.298	0.696	33.457	1.102	0.632	0.226
8.5	26.248	2.677	26.783	1.244	8.489	4.930	0.851	8.417	0.323	0.671	31.923	1.123	0.586	0.300
8.0	29.232	2.470	29.889	1.142	7.989	5.645	0.755	7.925	0.348	0.647	35.814	1.050	0.647	0.000
9.0	23.778	2.897	24.231	1.347	8.988	4.413	0.977	8.908	0.284	0.710	28.788	1.202	0.626	0.283
9.5	21.713	3.117	22.091	1.458	9.487	3.820	1.038	9.401	0.299	0.696	26.032	1.276	0.615	0.289
10.0	19.962	3.346	20.278	1.568	9.987	3.329	1.099	9.895	0.325	0.669	23.721	2.627	0.590	0.304
10.5	18.468	3.570	18.742	1.690	10.486	3.078	1.224	10.420	0.276	0.718	21.901	2.836	0.648	0.262
11.5	16.072	4.061	16.295	1.964	11.484	2.561	1.459	11.423	0.267	0.727	18.895	3.246	0.659	0.255
11.0	17.193	3.825	17.438	1.823	10.985	2.816	1.365	10.912	0.253	0.741	20.306	3.081	0.673	0.247
12.0	15.091	4.329	15.291	2.121	11.984	2.348	1.592	11.940	0.186	0.808	17.657	3.366	0.754	0.185
13.0	13.470	4.835	15.646	3.667	12.982	2.046	1.883	12.930	0.229	0.765	15.695	3.838	0.712	0.206
							$Z = 0.008$							
8.0	29.521	2.401	30.328	1.116	7.984	6.109	0.705	7.845	0.328	0.661	36.769	1.002	0.661	0.001
8.3	28.842	2.521	29.481	1.177	8.283	5.594	0.793	8.131	0.260	0.730	35.303	1.040	0.730	0.001
8.5	27.626	2.606	28.212	1.216	8.483	5.159	0.799	8.327	0.276	0.713	33.600	1.051	0.713	0.001
8.6	27.057	2.643	27.620	1.239	8.582	4.988	0.812	8.424	0.303	0.686	32.823	1.060	0.626	0.221
8.8	25.975	2.732	26.493	1.275	8.782	4.648	0.826	8.618	0.313	0.676	31.351	1.079	0.597	0.285
9.0	23.939	2.814	24.437	1.321	8.982	4.525	0.850	8.807	0.334	0.655	29.175	1.109	0.573	0.302
9.5	21.802	3.025	22.238	1.435	9.481	3.822	0.885	9.291	0.366	0.624	26.252	1.159	0.544	0.323

Table 1. continued.

$M_{\rm ini}$	$\tau_{\rm H}$	$m^{\rm H}_{\rm conv}$	$t_{\rm 1DUP}$	$m_{\rm 1DUP}$	$M_{\rm He}$	$\tau_{\rm He}$	$m^{\rm He}_{\rm conv}$	$M_{\rm HeBS}$	^{12}C	^{16}O	$t_{\rm 2DUP}$	$m_{\rm 2DUP}$	^{16}O	^{20}Ne
10.0	20.018	3.256	20.365	1.543	9.980	3.546	1.036	9.797	0.296	0.693	24.035	1.257	0.614	0.285
10.5	18.486	3.496	18.795	1.670	10.479	3.165	1.141	10.304	0.296	0.693	22.048	2.660	0.619	0.280
11.0	17.170	3.713	17.454	1.811	10.978	2.856	1.239	10.853	0.308	0.681	20.373	2.832	0.615	0.275
11.5	16.027	3.968	16.263	1.922	11.477	2.718	1.376	11.378	0.248	0.741	19.032	3.001	0.674	0.242
12.0	15.033	4.210	15.237	2.055	11.976	2.471	1.470	11.892	0.261	0.727	17.758	3.154	0.659	0.253
13.0	13.401	4.750	13.566	2.338	12.973	2.125	1.707	12.899	0.237	0.752	15.725	3.489	0.687	0.232
							$Z = 0.02$							
8.8	24.639	2.611	25.328	1.256	8.771	4.978	0.747	8.601	0.341	0.633	30.583	1.035	0.633	0.002
9.0	23.637	2.691	24.277	1.300	8.970	4.728	0.788	8.793	0.337	0.637	29.241	1.060	0.561	0.296
9.5	21.414	2.906	21.970	1.415	9.468	4.102	0.850	9.277	0.344	0.630	26.275	1.123	0.554	0.304
10.0	19.580	3.104	20.031	1.520	9.967	3.640	0.936	9.757	0.327	0.646	23.830	1.188	0.570	0.298
10.5	18.017	3.339	18.415	1.655	10.465	3.252	1.031	10.233	0.322	0.652	21.777	1.256	0.574	0.300
11.0	16.675	3.565	17.035	1.786	10.963	3.099	1.194	10.701	0.250	0.723	20.191	2.691	0.661	0.237
11.3	15.969	3.720	16.288	1.845	11.262	2.853	1.256	10.993	0.283	0.690	19.207	2.785	0.627	0.260
11.5	15.545	3.817	15.845	1.916	11.461	2.817	1.309	11.180	0.241	0.731	18.707	2.867	0.672	0.229
12.0	14.545	4.035	14.804	2.024	11.959	2.512	1.374	11.739	0.274	0.699	17.371	3.024	0.635	0.255
							$Z = 0.04$							
9.0	21.936	2.804	22.658	1.324	8.956	4.707	0.758	8.723	0.329	0.620	27.631	1.032	0.620	0.004
9.2	22.592	2.919	23.260	1.399	9.151	4.365	0.829	8.897	0.312	0.637	27.848	1.080	0.567	0.277
9.5	19.805	3.025	20.414	1.438	9.453	4.167	0.855	9.194	0.318	0.630	24.785	1.108	0.557	0.286
10.0	18.029	3.241	18.544	1.563	9.950	3.945	1.037	9.645	0.255	0.693	22.600	1.226	0.625	0.248
10.5	16.535	3.481	16.989	1.698	10.448	3.473	1.114	10.113	0.254	0.694	20.543	1.285	0.629	0.245
11.0	15.270	3.728	15.656	1.811	10.945	3.164	1.252	10.570	0.244	0.704	18.887	2.627	0.647	0.228
11.5	14.195	3.958	14.546	1.970	11.443	2.814	1.404	11.022	0.222	0.725	17.394	2.788	0.673	0.208
12.0	13.280	4.210	13.576	2.107	11.940	2.683	1.519	11.439	0.207	0.740	16.287	2.977	0.686	0.202
13.0	11.754	4.733	11.980	2.346	12.934	2.147	1.680	12.405	0.263	0.684	14.170	3.346	0.623	0.247
							overshooting $Z = 0.0001$							
5.0	88.374	1.495	89.541	0.853	4.999	10.336	0.673	4.996	0.348	0.651	100.115	0.971	0.651	0.000
5.5	72.004	1.682	80.929	1.651	5.499	8.143	0.688	5.496	0.349	0.651	81.223	1.025	0.651	0.000
5.7	63.004	1.769	71.374	1.715	5.699	7.658	0.746	5.696	0.334	0.666	71.635	1.051	0.666	0.000
6.0	60.145	1.890	67.390	1.818	5.999	6.633	0.797	5.996	0.318	0.682	67.625	1.104	0.601	0.289
7.0	44.299	2.284	49.256	2.140	6.998	4.545	0.982	6.996	0.335	0.664	49.408	1.249	0.578	0.318
7.5	38.879	2.492	43.171	2.322	7.498	3.952	1.094	7.496	0.316	0.684	43.291	1.341	0.605	0.297
8.0	34.503	2.708	38.276	2.501	7.998	3.485	1.217	7.995	0.299	0.701	38.371	2.585	0.629	0.279
9.0	28.006	3.157	30.984	2.875	8.998	2.769	1.476	8.995	0.283	0.717	31.050	2.988	0.645	0.270
10.0	23.433	3.621	25.887	3.258	9.998	2.292	1.763	9.995	0.268	0.731	25.936	3.384	0.666	0.250
							overshooting $Z = 0.02$							
7.0	47.648	1.936	49.458	1.174	6.964	6.422	0.740	6.757	0.318	0.655	56.083	1.042	0.656	0.002
7.5	41.177	2.134	42.728	1.301	7.461	5.304	0.824	7.228	0.322	0.651	48.194	1.126	0.583	0.278
8.0	36.611	2.324	37.333	1.432	7.959	4.545	0.993	7.695	0.312	0.661	41.989	1.213	0.591	0.279
8.5	32.419	2.522	33.043	1.569	8.457	3.953	1.046	8.162	0.302	0.671	37.076	1.291	0.600	0.280
8.8	30.565	2.641	31.113	1.674	8.754	3.603	1.113	8.428	0.302	0.671	34.785	1.356	0.600	0.282
8.9	29.919	2.682	30.464	1.691	8.854	3.558	1.177	8.514	0.277	0.696	34.093	2.198	0.635	0.252
9.0	29.317	2.717	29.819	1.730	8.953	3.483	1.211	8.602	0.266	0.707	33.359	2.439	0.644	0.250
9.1	28.671	2.757	29.198	1.743	9.053	3.347	1.180	8.704	0.291	0.683	32.614	2.479	0.618	0.266
9.3	27.259	2.844	27.730	1.794	9.253	3.254	1.215	8.893	0.288	0.685	31.034	2.558	0.620	0.265
9.5	26.370	2.916	26.844	1.877	9.451	3.089	1.287	9.061	0.270	0.703	29.978	2.643	0.640	0.252
10.0	23.866	3.150	24.234	1.991	9.950	2.813	1.459	9.522	0.263	0.710	27.087	2.819	0.646	0.249
10.5	22.031	3.367	22.345	2.160	10.446	2.467	1.575	9.951	0.280	0.693	24.848	3.008	0.627	0.263

Concerning the treatment of convection, we use the standard mixing length theory (with $\alpha = 1.75$ coming from solar fitting models) and the Schwarzschild criterion to delineate the convective boundaries. Instantaneous mixing is performed inside each convective zone at each iteration during the convergence process. For the models including core overshooting, mixing is treated as a diffusive process (Freytag et al. 1996; Blöcker et al. 1998) where the diffusion coefficient beyond the convective boundary is represented by an exponentially decreasing function of the radius given by $D(r > r_{\rm core}) = D_{\rm core} \times \exp\left[2(r_{\rm core} - r)/(f_{\rm over} \times H_{\rm P}^{\rm core})\right]$ depending on the parameter $f_{\rm over}$ where $r_{\rm core}$, $H_{\rm P}^{\rm core}$ and $D_{\rm core}$ are the radius, the pressure scale height and the convective diffusion coefficient at the edge of the core.

Core overshooting is generally invoked to account for the observed distribution of stars across the HR diagram (e.g. Schaller et al. 1992; Salasnich et al. 1999). Typical values of $f_{\rm over}$ range between ~0.01 and ~0.035 (e.g. Costa et al. 2006) and in our simulations, we opt for $f_{\rm over} = 0.016$. Note that overshooting is only applied at the edge of the convective core.

The initial solar composition is taken from Grevesse et al. (1996). For non-solar metallicities, the initial hydrogen mass fraction is given by $X = X_{\rm BB} + (X_\odot - X_{\rm BB})(Z/Z_\odot)$ where the primordial (Big Bang) value $X_{\rm BB} = 0.7521$ is taken from Coc et al. (2004). The initial mass fractions of metals are scaled from the solar values and the initial helium mass fraction is given by $Y = 1 - X - Z$. Below [Fe/H] = −0.5, the lithium abundance is set to the Spite plateau value of $n({\rm Li}) = 4.15 \times 10^{-10}$.

Starting from the pre-main sequence, computations were performed for 78 stellar models without overshooting with initial masses ($M_{\rm ini}$) $7 \leq M_{\rm ini}/M_{\odot} \leq 13$ and initial metallicities $Z = \{10^{-5}, 10^{-4}, 10^{-3}, 0.008, 0.004, 0.02, 0.04\}$, and a grid of 21 stellar models with core overshooting, having $5 \leq M_{\rm ini}/M_{\odot} \leq 10.5$ and $Z = \{10^{-4}, 0.02\}$.

3. Evolutionary properties up to the end of carbon burning

In this section, we discuss some evolutionary properties of SAGB stars up to the end of the carbon burning phase where the computations were (temporarily) stopped. All the models and tables can be retrieved on the author's website at `http://www-astro.ulb.ac.be/~siess/database.html`. Additional material including the surface composition at the end of the first and second dredge-up is also available online in the electronic version of this paper. Comparisons with existing models (mostly solar) as well as the effects of varying the physical inputs can be found in Paper I and are not reproduced here.

3.1. H and He burning phases

Up to core helium exhaustion, the evolution of SAGB stars is very similar to that of intermediate mass stars. H burning takes place in a convective core and is followed by the deepening of the convective envelope during the first dredge-up (1DUP). Then, when the central temperature reaches 10^8 K, He ignites and convection resumes in the core.

An interesting feature in relation to the fate of SAGB stars is the dependence of the maximum size of the convective core (during central H and He burning) on metallicity (Fig. 1). Similar to their lower mass counterparts (Chieffi & Tornambè 1986; Cassisi & Castellani 1993), the convective core of SAGB stars during central H and He burning reaches a maximum extent around $Z = 10^{-4}$. This behavior is attributed to the fact that with decreasing metallicity, the star develops higher central temperatures to compensate for the decrease of nuclear energy production associated with a lower CNO content and larger radiative losses from the surface (the envelope opacity decreases with Z and the luminosity increases). As explained in Chieffi & Tornambè (1986), when the metallicity approaches 10^{-4}, these effects reach saturation: the contribution of metals to the opacity vanishes and the nuclear energy production, partially transferred to the pp chains, becomes less centrally confined. Below $Z = 10^{-4}$, the structure does not change much but the nuclear energy production slightly decreases because $Z_{\rm CNO}$ decreases. As a result, the core mass decreases below $Z \simeq 10^{-4}$.

Contrary to the previous trend, the metal rich $Z = 0.04$ models develop more massive H convective cores than their solar counterparts. This exception is related to the variation of the initial helium content with metallicity. Indeed, as Z spans three orders of magnitude from 10^{-5} to $Z = 0.02$, Y increases by only 0.02 in mass fraction (8%) while in the metallicity range $Z = 0.02$–0.04, it increases by 11%, passing from 0.27 to 0.30. Such a large helium enrichment overwhelms the opacity effect associated with the metal enhancement and the envelope opacity globally decreases. As a result, the star develops a larger convective core during the H-burning (see also Bono et al. 2000).

The core properties during central He burning are inherited from those established during the main sequence (Fig. 1) and logically the size of the He core reaches a maximum around $Z \simeq 10^{-4}$ and a minimum near the solar value. Note however that for the $Z = 0.04$ models, this increase in the core mass only affects stars with $M_{\rm ini} \gtrsim 9.5\ M_{\odot}$.

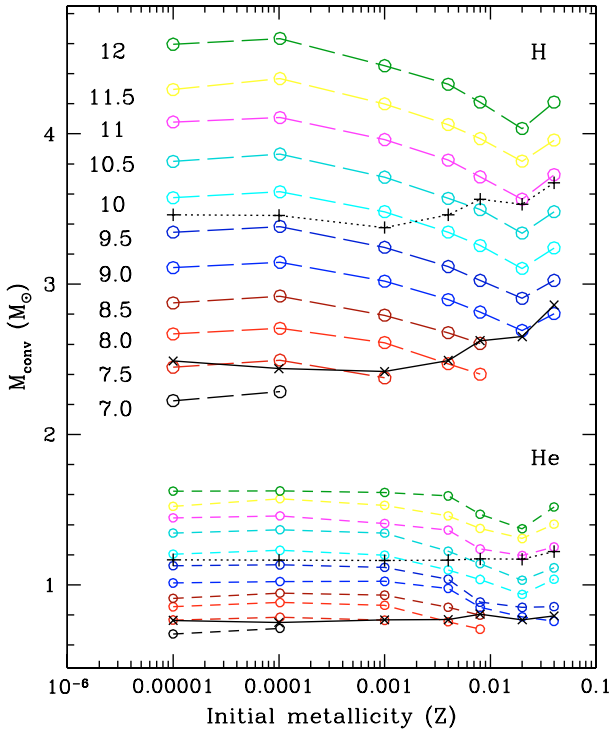

Fig. 1. Maximum mass of the convective core during the central H (long-dashed lines) and He (short dashed) burning phases as a function of metallicity for the models without overshooting. The initial stellar mass is indicated in front of each curve for the H convective cores and is not repeated for the He burning cores. Crosses (×) and plus signs (+) connected by solid and dotted lines represent the convective core masses corresponding to $M_{\rm up}$ and $M_{\rm mas}$, respectively.

At H ignition, a convective core develops that rapidly reaches its maximum extent as the CN cycle comes to equilibrium. During the main sequence, overshooting does not substantially increase the maximum core size but it does contribute to replenishing the central burning regions with the unburnt H that surrounds the convective zone. As a result, convection recedes more slowly, leading to a longer main sequence ($\tau_{\rm H}$) lifetime.

The situation is however different during central He burning because the layers surrounding the core are dynamically unstable. In this case convection grows in mass as burning proceeds and overshooting has a greater impact. As can be seen from Table 1 the core mass is increased by 0.3 to 0.6 $M_{\odot}$. Because the stellar luminosity is higher (bigger cores generate more energy), the duration of the He-burning phase ($\tau_{\rm He}$) is shortened and the ratio $\tau_{\rm He}/\tau_{\rm H}$ is about a factor of 1.5 to 2.5 lower than in the models without overshooting. By increasing the He core size, overshooting makes the star behave as if it was initially more massive.

Like intermediate-mass stars of the same composition, all our models with $Z > 0.001$ experience the 1DUP and, in the HR diagram, the star moves to the red giant branch (RGB), burning hydrogen in a shell above a contracting core essentially made of ^{4}He (central mass fraction ~0.96–0.99). Below $Z \leq 0.001$, because of the higher internal temperature of metal poor stars, He ignites soon after central H exhaustion and the 1DUP is avoided. The presence of overshooting does not affect this evolutionary feature.

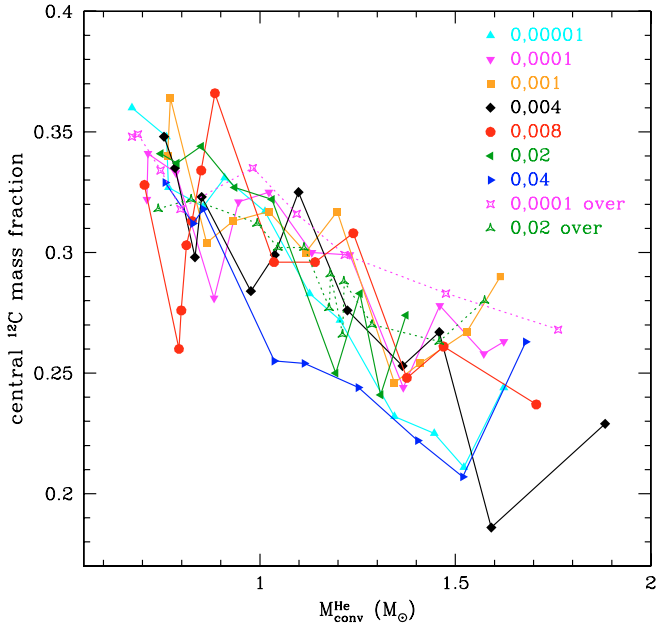

Fig. 2. Central ^{12}C mass fraction at the end of He burning as a function of the convective He core mass ($M_{\rm He}^{\rm conv}$) for the different metallicities.

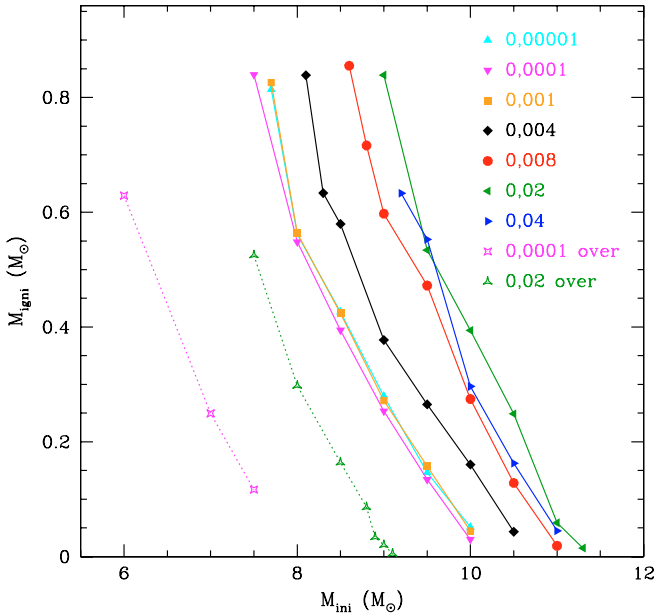

Fig. 3. Mass coordinate of carbon ignition ($m_{\rm igni}$) as a function of initial mass for the different considered metallicities. The dotted lines refer to models with overshooting.

For models where the 1DUP takes place, surface composition changes (Table 4) are similar to those of lower-mass stars: the hydrogen mass fraction decreases to the benefit of ^{4}He, ^{13}C, ^{14}N and ^{17}O while ^{12}C, ^{15}N and ^{16,18}O are depleted, leading to a decrease of the ^{12}C/^{13}C ratio from ~90 to ~20 (Paper I). The slight surface enrichment in ^{23}Na and ^{21}Ne concomitant with a decrease of ^{22}Ne reflects the partial activation of the NeNa chain. Given the (relatively) low temperature ($<5-6\times10^{7}$ K) of the H burning shell (HBS), the MgAl chain is marginally activated, yielding a small destruction of ^{25}Mg and increase in ^{26}Mg (Arnould et al. 1999). Note that the presence of extra mixing at the base of the convective envelope (not taken into account in these simulations) would exacerbate the chemical modifications and contribute for example to further decrease the ^{12}C/^{13}C ratio as observed (e.g. Charbonnel 2006).

Nucleosynthesis during core He burning leads primarily to the production of ^{12}C and ^{16}O via the 3α and ^{12}C$(\alpha,\gamma)^{16}$O reactions respectively and also to the conversion of ^{14}N into ^{22}Ne by the reaction chain ^{14}N$(\alpha,\gamma)^{18}$F$(\beta^{+})^{18}$O$(\alpha,\gamma)^{22}$Ne. The central ^{12}C abundance strongly anti-correlates with the core mass implying that more massive cores develop higher internal temperatures (Fig. 2). Consequently the C/O ratio in the core decreases with increasing initial mass and thus if overshooting is present. Typical values (expressed in terms of the mass fraction ratio) range between ~0.3 and ~0.6, in agreement with the calculations of Straniero et al. (2003). Now, if we analyze the behavior of the central abundances of C, O or of the C/O ratio with metallicity when the initial mass is fixed, no clear trend emerges from our simulations. A reason for this lack of correlation may be related to the fact that, as pointed out by Imbriani et al. (2001), the final O abundance is very sensitive to the evolution of the core properties near the end of central He burning which obviously does not depend linearly on composition. Furthermore, as discussed in Sect. 4.1, the modeling of core He burning is subject to large uncertainties associated with the unstable nature of the convective boundaries. All these considerations make the determination of the C/O ratio as a function of Z highly uncertain (Imbriani et al. 2001). Models with overshooting develop more massive and hotter cores. As a consequence, for a given $M_{\rm ini}$, they favor the ^{12}C$(\alpha,\gamma)^{16}$O reactions and thus the depletion of ^{12}C.

3.2. The C-burning phase

At central He exhaustion, the temperature maximum $T_{\rm max}$ increases and moves outward as a consequence of neutrino emission. In stars with $M \geq M_{\rm up}$, the peak temperature reaches $T_{\rm max} \sim 6-6.5\times10^{8}K$ and carbon ignites off-center. As shown in Fig. 3, the mass coordinate of C-ignition $m_{\rm igni}$ is a decreasing function of $M_{\rm ini}$. This is simply explained by the fact that, with increasing core mass, the central degeneracy is lower and the star maintains its maximum temperature closer to the center. This also implies that C ignites at a smaller radius (thereafter $r_{\rm igni}$) when $M_{\rm ini}$ increases. The dependence of $m_{\rm igni}$ on metallicity is essentially linked to the opacity effects that affected the core mass during the central H and He burning phases. Thus, for a given initial mass, $m_{\rm igni}$ presents a minimum around $Z = 10^{-4}$ and a maximum around $Z = 0.02$. This conclusions also holds if core overshooting is considered. The main difference is that the minimum mass for carbon ignition is lowered by ~2 $M_{\odot}$ in the overshoot models (see Sect. 4.1).

Once carbon ignites, the evolution proceeds in two steps (Siess 2006a,b): first a convective carbon flash which induces a structural re-adjustment leading to a temporary quenching of the convective instability and then the development of a convective flame which propagates to the stellar center (Fig. 4). Selected evolutionary properties during the C-burning phase are presented in Table 2.

The strength of the carbon flash ($L_{C_{\rm max}}^{\rm flash}$ which measures the nuclear luminosity in the C-burning shell) is essentially determined by the state of degeneracy of the plasma at the ignition point. Lower mass stars develop higher core degeneracy and generate stronger flashes. The duration of the flash ($\tau_{\rm flash}$) does not always correlate with the flash intensity. As explained in Paper I, this is due to the fact that $\tau_{\rm flash}$ depends on the rate at which ^{12}C is depleted which in turn depends on the initial carbon

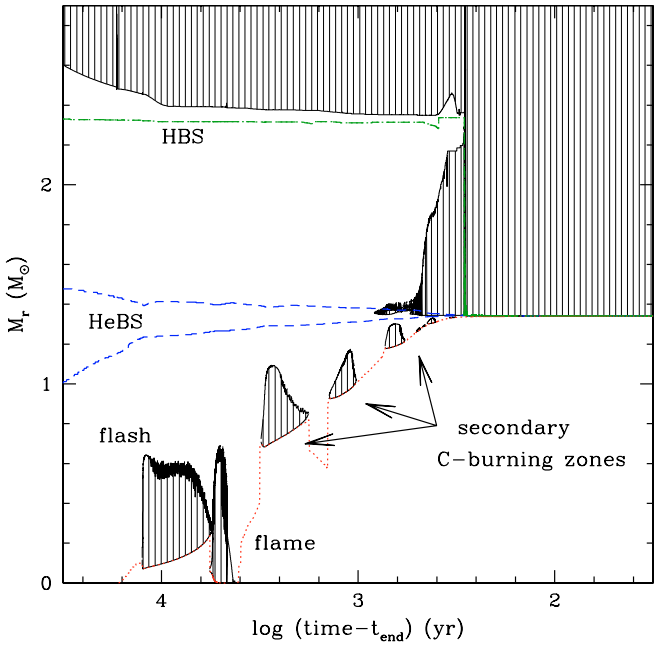

Fig. 4. Kippenhahn diagram showing the evolution of internal structure during the carbon burning phase and illustrating the dredge-out phenomenon. The model is a 7.5 $M_\odot$, $Z = 10^{-4}$ stellar model computed with overshooting. The hatched areas correspond to convective zones. On the x-axis, the time is counted backward from the last computed model ($t_{\rm end}$).

abundance in the core, on the thermodynamical conditions in the flash and on the extent of the convective instability ($\Delta m_{\rm flash}$). This is why there is not a simple one-to-one correlation between $\tau_{\rm flash}$ and $\Delta m_{\rm flash}$.

The time needed for the flame to reach the center $\tau_{\rm flame}$ depends on how far out (in radius) it ignites and on its velocity. Timmes et al. (1994) showed that the deflagration speed is proportional to T^{14}, where the temperature T is evaluated at the base of the burning front. The flame will consequently propagate more rapidly in models with higher internal temperatures, i.e. in stars with more massive cores, which also have the smaller $r_{\rm igni}$. By increasing the core mass, overshooting contributes to lower $\tau_{\rm flame}$. Comparisons of the flame speed with previous studies (Paper I) indicate a relatively good agreement (at least at solar metallicity where numbers are available). Note that a good estimate of the flame speed is given by $v_{\rm flame} = r_{\rm flame}/\tau_{\rm flame}$, where $r_{\rm flame}$ and $\tau_{\rm flame}$ can be found in Table 2. Typical values are in the range 10^{-3}–10^{-2} cm s^{-1}.

Finally, in the most massive stars where the carbon flash ignites very close to the center, for $m_{\rm igni} \lesssim 0.05\ M_\odot$, there is only one convective episode and no flame (e.g. 11 $M_\odot$ with $Z = 0.008$, 11.3 $M_\odot$ with $Z = 0.02$, 11 $M_\odot$ with $Z = 0.04$ and the two $Z = 0.02$ models with overshooting having $M_{\rm ini} = 9.0$ and 9.1 $M_\odot$).

C-burning proceeds through the ^{12}C(^{12}C,α)^{20}Ne and ^{12}C(^{12}C,p)^{23}Na reactions and is complemented by the ^{16}O(α,γ)^{20}Ne reaction. These reactions convert the core into an ONe mixture made of ^{16}O (∼50–70%) and ^{20}Ne (∼15–35%) with traces of ^{23}Na (∼3–5%), ^{24}Mg (∼2–3%), ^{25}Mg (∼0.3–2%), ^{26}Mg (∼0.2–1%), ^{22}Ne (∼0.1–1%), ^{21}Ne (∼0.3–0.5%), ^{27}Al (∼0.1–0.8%) and ^{17}O (∼0.001–0.008%).

^{23}Na appears as the third most abundant nuclide in the core thus yielding to the formation of an ONeNa WD, in agreement with the computations of Ritossa et al. (1996). The case of ^{24}Mg is interesting because the heat released by electron capture reactions on this element during a subsequent EC-SN event may be able to raise the temperature above the threshold for explosive oxygen burning, thus affecting the hydrodynamical collapse. However, the abundance of ^{24}Mg found in our models is always too small (by a factor ∼10) compared to that required to produce an explosion able to disrupt the SAGB star (Gutiérrez et al. 2005).

Similarly, ^{12}C can play an important role in the explosion if the conditions for core collapse are reached. According to the numerical simulations of Gutiérrez et al. (2005), traces of unburnt ^{12}C as small as ≃1.5% by mass are sufficient to ignite a thermonuclear SN (as in Type Ia) which will reverse the collapse and disrupt the core. This threshold core carbon abundance is exceeded in some of the lowest mass models ($M = \{8\}$, $Z = \{10^{-4}, 10^{-3}\}$; $M = \{8.1, 8.3\}$, $Z = \{0.004\}$; $M = \{8.6, 8.8, 9.0\}$, $Z = 0.008$; $M = \{7.5\}$, $Z = \{0.02$ and overshooting$\}$) which are not expected to follow this explosive evolutionary path, unless of course a companion is present.

The central ^{20}Ne and ^{16}O abundances are of primary nature and thus metallicity independent. For increasing core mass, ^{20}Ne decreases. We also note that ^{20}Ne+^{16}O is almost constant, ranging between 0.87 and 0.92. The central O/Ne ratio varies between ∼1.5 and ∼3.5 and similarly to the C/O ratio at the end of core He burning, no clear correlation with metallicity can be established.

3.3. Evolution up to the beginning of the TP-SAGB phase

The time of occurrence of the second dredge-up depends on the stellar evolutionary timescale. With increasing mass, the time interval between central He exhaustion and carbon ignition reduces. In SAGB stars it becomes shorter than the time needed for the convective envelope to reach its deepest extent and the completion of the second dredge-up (2DUP) is postponed either at the beginning, during or at the end of the C-burning phase (e.g. Siess 2006a). As studied by Iben et al. (1997), the onset of C-burning hinders the inward penetration of the envelope which further delays the realization of this deep mixing event. In summary, the 2DUP occurs later in the evolution as the mass increases or if core overshooting is taken into account.

A unique feature of SAGB evolution is the ability for the models with initial masses close to $M_{\rm mas}$ to experience the so-called "dredge-out" event (Iben et al. 1997; Siess 2006b; Siess & Pumo 2006c). This phenomenon occurs near the end of the C-burning phase when the 2DUP comes to completion. It is characterized by the formation of a convective zone in the HeBS which grows outward in mass and merges with the descending convective envelope (Fig. 4). Dredge-out is present in the following models: 9.5 $M_\odot$ with $Z = \{10^{-5}, 10^{-4}, 10^{-3}\}$, 10 $M_\odot$ with $Z = \{0.008, 0.004\}$, 10.8 $M_\odot$ with $Z = 0.02$, 7.5 $M_\odot$ with overshooting and $Z = 10^{-4}$ and is responsible for a large surface enrichment in ^{4}He and ^{12}C, leading to the formation of a C-rich star.

Concerning the modifications to the surface abundances, it is important to note the existence of a critical initial mass, hereafter referred to as $M_{\rm 2DUP}$ (see Sect. 6 for details), above which the 2DUP does not lead to a reduction of the H-free core. For SAGB stars in the mass range $M_{\rm up} \lesssim M_{\rm ini} \lesssim M_{\rm 2DUP}$, the envelope penetrates below the HBS and leads to a potentially large surface helium enrichment by 40–50% compared to the 1DUP value (Table 4 vs. 5). Aside from this main feature, the chemical signatures of the 2DUP are similar to those affecting the star

Table 2. Selected evolutionary features during the C-burning phase as a function of $M_{\rm ini}$. The quantities shown are: the time ($t_{\rm igni}$ in 10^7 yr) and stellar mass ($M_{\rm igni}$ in $M_\odot$) at C-ignition, the radius ($r_{\rm igni}$ in km) and mass coordinate ($m_{\rm igni}$ in $M_\odot$) of C-ignition, the degeneracy at that location ($\eta_{\rm flash}$), the maximum carbon luminosity during the flash ($L^{\rm flash}_{C_{\rm max}}$ in $L_\odot$), the duration of the flash ($\tau_{\rm flash}$ in yr), the mass covered by the convective instability during the flash ($\Delta m_{\rm flash}$), the radius ($r_{\rm flame}$ in km) and mass coordinate ($m_{\rm flame}$ in $M_\odot$) where the flame develops, the maximum carbon luminosity during the flame ($L^{\rm flame}_{C_{\rm max}}$ in $L_\odot$) and the duration of the flame ($\tau_{\rm flame}$ in yr). When carbon ignites at the center ($r_{\rm flash}=0$) $\Delta m_{\rm flash}$ corresponds to the maximum extent of the convective C-burning core.

$M_{\rm ini}$	$t_{\rm igni}$	$M_{\rm igni}$	$r_{\rm igni}$	$m_{\rm igni}$	$\eta_{\rm flash}$	$L^{\rm flash}_{C_{\rm max}}$	$\tau_{\rm flash}$	$\Delta m_{\rm flash}$	$r_{\rm flame}$	$m_{\rm flame}$	$L^{\rm flame}_{C_{\rm max}}$	$\tau_{\rm flame}$
						$Z=0.00001$						
7.7	3.581	7.698	4266	0.814	2.609	1.160(8)	190	0.268	4184	0.725	1.280(7)	15605
8.0	3.288	7.998	4199	0.561	2.541	1.284(7)	695	0.447	5075	0.508	2.558(5)	8440
8.5	2.949	8.498	4066	0.426	2.623	5.127(6)	1641	0.506	4660	0.387	4.018(5)	8170
9.0	2.673	8.998	3763	0.280	2.600	1.964(6)	5590	0.554	3629	0.233	7.332(5)	2285
9.5	2.442	9.498	3191	0.147	2.638	9.731(5)	5203	0.571	2944	0.105	3.127(5)	802
10.0	2.250	9.998	2315	0.051	2.670	6.664(5)	5162	0.576	2143	0.035	1.283(5)	427
10.5	2.085	10.498	0	0.000	1.810	3.242(5)	2447	0.521				
11.0	1.936	10.997	0	0.000	1.614	2.451(5)	3601	0.560				
11.5	1.862	11.498	0	0.000	1.470	1.850(5)	2967	0.538				
12.0	1.700	11.998	0	0.000	0.720	1.568(5)	2438	0.512				
						$Z=0.0001$						
8.0	3.346	7.997	4174	0.548	2.618	1.081(7)	503	0.449	5060	0.494	1.855(5)	7289
8.5	2.994	8.497	4037	0.394	2.582	3.890(6)	1988	0.496	4647	0.325	1.894(5)	5139
9.0	2.708	8.997	3648	0.253	2.591	1.841(6)	6074	0.557	3483	0.211	7.062(5)	2150
9.5	2.474	9.497	3121	0.134	2.630	8.981(5)	5920	0.571	2809	0.092	3.475(5)	743
10.0	2.274	9.996	1984	0.030	2.451	5.349(5)	6377	0.587	1354	0.008	4.864(4)	365
10.5	2.182	10.496	0	0.000	2.512	2.661(5)	4222	0.557				
11.0	2.018	10.996	0	0.000	1.585	1.745(5)	5115	0.584				
11.5	1.895	11.496	0	0.000	1.870	1.490(5)	4148	0.583				
12.0	1.723	11.995	0	0.000	1.732	1.247(5)	4260	0.602				
						$Z=0.001$						
7.7	3.696	7.684	4173	0.826	2.563	1.735(8)	311	0.256	4440	0.739	5.029(6)	15009
8.0	3.450	7.984	4132	0.563	2.586	1.343(7)	543	0.442	5068	0.521	2.407(5)	8308
8.5	3.172	8.483	4038	0.424	2.703	5.107(6)	1702	0.508	4568	0.384	4.212(5)	7493
9.0	2.780	8.983	3731	0.272	2.660	1.921(6)	5431	0.556	3623	0.223	6.158(5)	2337
9.5	2.531	9.483	3264	0.157	2.641	1.006(6)	5830	0.569	2997	0.115	3.886(5)	835
10.0	2.392	9.982	2232	0.044	2.642	5.948(5)	8017	0.596	1740	0.022	2.150(5)	250
10.5	2.148	10.481	0	0.000	1.777	2.902(5)	2819	0.525				
11.0	1.996	10.981	0	0.000	1.501	2.221(5)	2976	0.521				
11.5	1.860	11.481	0	0.000	1.044	1.666(5)	3056	0.526				
12.0	1.804	11.980	0	0.000	1.699	1.324(5)	4971	0.618				
						$Z=0.004$						
8.1	3.498	8.023	4149	0.839	2.480	1.846(8)	194	0.237	4491	0.798	3.536(7)	13401
8.3	3.343	8.219	4116	0.633	2.600	1.101(8)	562	0.398	4351	0.584	1.044(7)	10276
8.5	3.190	8.417	4219	0.580	2.560	1.396(7)	612	0.435	5104	0.523	2.777(5)	8900
9.0	2.877	8.908	3958	0.377	2.574	3.498(6)	1664	0.499	4570	0.317	1.585(5)	4029
9.5	2.602	9.401	3717	0.265	2.628	1.785(6)	4559	0.558	3687	0.212	4.188(5)	2554
10.0	2.371	9.895	3288	0.160	2.638	1.015(6)	6800	0.568	2911	0.111	4.982(5)	861
10.5	2.189	10.420	2215	0.043	2.510	5.827(5)	5552	0.580	1667	0.017	8.204(4)	308
11.5	1.889	11.423	0	0.000	1.466	2.549(5)	4085	0.564				
11.0	2.030	10.912	0	0.000	1.674	2.538(5)	2996	0.522				
12.0	1.765	11.927	0	0.000	1.360	6.269(5)	2134	0.515				
13.0	1.569	12.917	0	0.000	0.106	1.447(5)	1805	0.509				
						$Z=0.008$						
8.6	3.283	8.422	4062	0.855	2.821	3.304(8)	336	0.228	4825	0.786	1.293(6)	12625
8.8	3.135	8.617	4044	0.716	2.729	1.739(8)	232	0.351	1671235	0.580	2.139(6)	9609
9.0	2.915	8.807	4186	0.597	2.602	1.789(7)	612	0.424	5182	0.544	2.769(5)	9994
9.5	2.623	9.291	4167	0.472	2.680	7.001(6)	1384	0.414	4703	0.423	5.504(5)	11123
10.0	2.402	9.797	3758	0.275	2.672	1.846(6)	4471	0.555	3722	0.219	4.357(5)	2846
10.5	2.204	10.304	3087	0.128	2.644	8.446(5)	5968	0.586	2701	0.083	3.226(5)	615
11.0	2.036	10.851	1716	0.019	2.404	5.035(5)	6955	0.587				
11.5	1.903	11.377	0	0.000	1.632	2.454(5)	2901	0.519				
12.0	1.775	11.891	0	0.000	1.280	1.863(5)	3132	0.523				
13.0	1.572	12.890	0	0.000	0.502	1.453(5)	2249	0.507				
						$Z=0.02$						
9.0	2.924	8.793	4220	0.839	2.684	1.803(8)	248	0.238	4256	0.752	1.090(7)	14207
9.5	2.625	9.277	4168	0.534	2.719	1.493(7)	868	0.453	4700	0.493	1.223(6)	11584
10.0	2.381	9.757	4051	0.394	2.726	5.331(6)	3287	0.480	4461	0.341	6.539(5)	7318

Table 2. continued.

$M_{\rm ini}$	$t_{\rm igni}$	$M_{\rm igni}$	$r_{\rm igni}$	$m_{\rm igni}$	$\eta_{\rm flash}$	$L^{\rm flash}_{C_{\rm max}}$	$\tau_{\rm flash}$	$\Delta m_{\rm flash}$	$r_{\rm flame}$	$m_{\rm flame}$	$L^{\rm flame}_{C_{\rm max}}$	$\tau_{\rm flame}$
10.5	2.176	10.233	3678	0.249	2.724	2.295(6)	6740	0.559	3308	0.191	1.177(6)	1651
11.0	2.018	10.700	2414	0.059	2.587	9.624(5)	4743	0.569	2045	0.032	1.577(5)	413
11.3	1.920	10.993	1586	0.015	2.306	7.209(5)	5011	0.569				
11.5	1.870	11.180	0	0.000	1.869	4.585(5)	3728	0.552				
12.0	1.736	11.739	0	0.000	1.639	3.076(5)	4616	0.560				
						$Z = 0.04$						
9.2	2.783	8.897	4097	0.633	2.827	5.044(7)	399	0.401	4461	0.596	4.056(6)	10970
9.5	2.476	9.194	4203	0.553	2.639	1.138(7)	784	0.423	5046	0.493	2.625(5)	8732
10.0	2.259	9.645	3777	0.296	2.660	1.962(6)	1960	0.526	4184	0.239	1.546(5)	2586
10.5	2.054	10.113	3215	0.163	2.642	1.081(6)	2822	0.553	3338	0.122	1.452(5)	1284
11.0	1.888	10.570	2225	0.045	2.436	5.835(5)	3026	0.567				
11.5	1.739	11.022	0	0.000	1.527	3.009(5)	3670	0.538				
12.0	1.628	11.439	0	0.000	1.028	1.783(5)	2131	0.489				
13.0	1.417	12.356	0	0.000	0.495	1.286(5)	2913	0.538				
						overshooting $Z = 0.0001$						
6.0	6.760	5.996	4144	0.629	2.748	3.584(7)	420	0.416	4480	0.578	2.756(6)	10520
7.0	4.939	6.996	3620	0.250	2.758	2.604(6)	6856	0.562	3396	0.210	1.461(6)	2432
7.5	4.328	7.496	3037	0.117	2.774	1.123(6)	6858	0.574	2464	0.062	5.043(5)	1394
8.0	3.836	7.995	0	0.000	2.109	5.051(5)	5615	0.569				
9.0	3.104	8.995	0	0.000	0.900	1.976(5)	4455	0.579				
10.0	2.593	9.995	0	0.000	0.084	1.629(5)	3264	0.604				
						overshooting $Z = 0.02$						
7.5	4.817	7.228	4126	0.525	2.810	1.573(7)	821	0.467	4603	0.466	8.417(5)	9908
8.0	4.197	7.695	3724	0.298	2.725	3.541(6)	4298	0.522	4030	0.266	4.553(5)	4371
8.5	3.706	8.162	3272	0.164	2.761	1.483(6)	5956	0.566	3005	0.120	6.029(5)	1480
8.8	3.477	8.428	2778	0.086	2.763	9.366(5)	6817	0.569	2086	0.037	3.514(5)	1129
8.9	3.408	8.514	2042	0.034	2.468	8.003(5)	5788	0.569	1520	0.012	8.799(4)	385
9.0	3.335	8.602	1740	0.020	2.270	7.105(5)	4705	0.592				
9.1	3.261	8.704	1055	0.005	2.243	6.052(5)	5698	0.593				
9.3	3.103	8.893	0	0.000	1.936	3.991(5)	5427	0.562				
9.5	2.997	9.060	0	0.000	1.583	2.974(5)	4746	0.559				
10.0	2.708	9.522	0	0.000	1.099	2.189(5)	4277	0.563				
10.5	2.484	9.951	0	0.000	0.671	1.752(5)	4310	0.585				

during the 1DUP as in both cases the ashes of H burning are brought to the surface. We note however a slightly larger contribution from the elements participating in the NeNa and MgAl chains. In stars with $M_{\rm ini} \geq M_{\rm 2DUP}$, the surface composition changes are small due to the fact that the envelope engulfs a region that was previously homogenized with the products of H-burning during the first dredge-up. The only noticeable exceptions are the low metallicity models ($Z \leq 0.001$) which did not experience the 1DUP. Because of their low initial metal content, surface enrichment can be large. For instance, in the $Z = 10^{-5}$ models, the ^{12}C abundance can be multiplied by a factor 10 to 200 depending on the initial mass, but these mass fractions remain anyway relatively low. Table 5 provides the surface mass fractions of the main elements at the end of the second dredge-up.

After completion of the 2DUP and extinction of carbon burning, the stellar luminosity is almost entirely supplied by the HeBS since H burning is switched-off during the 2DUP. The core is now strongly degenerate and isothermal and does not contribute significantly to the release of gravothermal energy. During the so called "early-AGB phase", the convective envelope retreats and the HeBS advances in mass until it approaches the H-He discontinuity. There, it loses its efficiency and allows the overlying layers to contract and re-heat. The HBS then reignites and the star enters the TP-SAGB phase. Details of this evolution as well as of the nucleosynthesis will be provided in a forthcoming paper, however some features can already be anticipated from Siess (2006b, 2007).

4. Mass transitions

In this section, we determine and analyze the different limiting masses and, in the first place $M_{\rm up}$, the minimum mass for carbon ignition.

4.1. The mass transition M_{up}

For each metallicity, the value of $M_{\rm up}$ was estimated by taking the mean between the initial mass of the least massive model that ignites carbon and the initial mass of the most massive model that does not. A typical error equal to half of the difference between these 2 limiting values was then assigned. It is important to stress that this error does not represent the true uncertainty on the value of $M_{\rm up}$ which, in reality, is much larger. A realistic estimate of this uncertainty should take into account the effects associated with the use of different physical inputs or numerical schemes/resolutions. In a recent paper, Poelarends et al. (2007) showed that the main source of uncertainty affecting the initial mass range of SAGB stars comes from the treatment of semiconvection and convective overshooting. Using three different stellar evolution codes characterized by three different mixing prescriptions, they found that $M_{\rm up}$ varies between 7.5 and 9.0 $M_\odot$ for the same initial composition.

The ability for a star to ignite carbon depends primarily on its CO core mass. If it is too small, the heat released by core contraction at the end of central He burning is not sufficient to overcome the energy lost by the neutrinos and the threshold

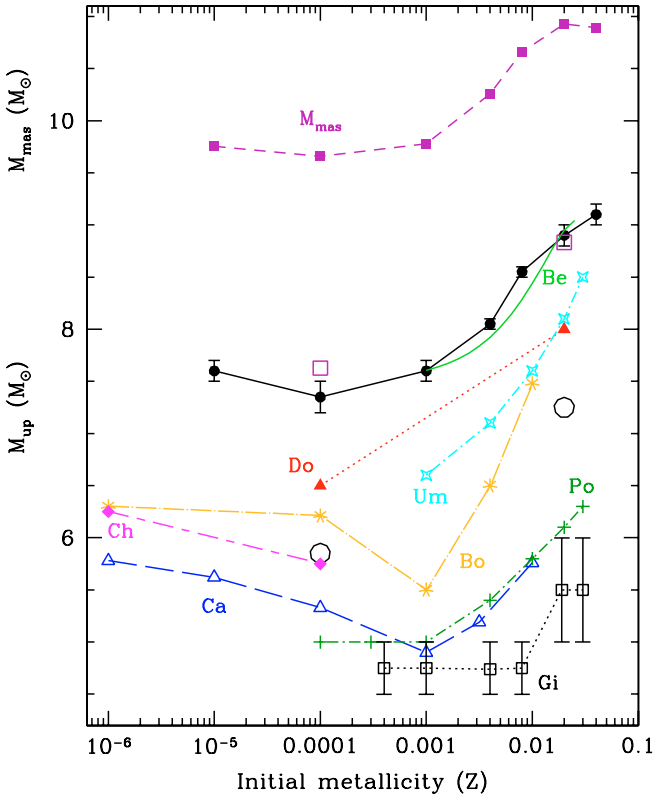

Fig. 5. Transition mass $M_{\rm mas}$ (filled squares connected by a dashed line) and $M_{\rm up}$ (dots connected by a solid line) as a function of Z. The values of $M_{\rm mas}$ and $M_{\rm up}$ for the models with overshooting are represented by big open squares and circles, respectively. Results of $M_{\rm up}$ from other studies are also displayed: Do (Dominguez et al. 1999), Um (Umeda et al. 1999), Bo (Bono et al. 2000), Ca (Cassisi & Castellani 1993), Ch (Chieffi & Tornambè 1986), Be (Becker & Iben 1979), Gi (Girardi et al. 2000), Po (Pols et al. 1998).

temperature for C-ignition cannot be reached. This is why the behavior of $M_{\rm up}$ with metallicity is similar to that of the convective core during He burning, showing for stars with $M_{\rm ini} \leq 9.5\ M_\odot$ only one extrema around $Z = 10^{-4}$ (Fig. 5).

Our "standard" values of $M_{\rm up}$ computed without overshooting are generally larger by 0.5–2 $M_\odot$ compared with other data using the same treatment of mixing (Dominguez et al. 1999; Umeda et al. 1999; Bono et al. 2000) except for the Becker & Iben (1979) models where the agreement is quite good. The origin of the differences is difficult to determine because it involves evolutionary sequences obtained by means of different evolutionary codes with different input physics and not all the authors provide a full description of the numerical algorithm used in their simulations. The situation is further complicated by the fact that the value of $M_{\rm up}$ critically depends on the size of the He burning core which is extremely sensitive to both numerical and physical inputs. In our calculations, special attention was paid to prevent any kind of diffusion at the Schwarzschild boundary, allowing us to precisely determine the effect of extra-mixing when it is incorporated in the computation. It is not within the scope of this paper to describe the numerical treatment of core He burning and its effects on the structure, however we simply mention one numerical experiment: if, in the algorithm for grid definition which is called at the beginning of each new time step, we allow the addition or removal of a shell located precisely at the convective interface, because we do not know the composition that must be assigned to this new mesh point, we inevitably introduce some diffusion. This numerical diffusion then propagates and because the layers surrounding the convective He core are unstable to semiconvection (e.g. Straniero et al. 2003, for a recent discussion), we end up forming a core $\gtrsim$0.1 $M_\odot$ more massive, corresponding to an equivalent increase of >0.5 $M_\odot$ in $M_{\rm ini}$. This example illustrates how difficult it is to determine precisely the extent of the convective region during central He burning and how it depends on apparently insignificant technical details. Our "conservative" approach minimizes mixing and, as such, we logically end up with the smallest He cores i.e. the highest values for $M_{\rm up}$.

This comparison also shows that the minimum in $M_{\rm up}$ varies between $Z \approx 10^{-3}$ (Bono et al. 2000; Cassisi & Castellani 1993) and $Z \approx 10^{-4}$ in the models of Dominguez et al. (1999) and in ours. We note however that the computations of Bono et al. (2000) assume a lower initial He abundance of $Y = 0.23$ for $Z < 0.01$ compared to ~0.245 in our models. This difference can account for a vertical shift of $M_{\rm up}$ (He rich stars develop more massive cores) but hardly explains the metallicity offset. This mass shift is quite surprising since Dominguez et al. (1999) use the same code and initial composition as Bono et al. (2000) but find a minimum in $M_{\rm up}$ around $Z = 10^{-4}$.

Overshooting represents an extension of mixing beyond the formal convective boundary and leads to an increase in the core size. This process makes the star behave as if it was initially more massive and $M_{\rm up}$ is consequently lowered by ~1.5–2 $M_\odot$, passing from $7.25 \pm 0.25\ M_\odot$ to $5.75 \pm 0.25\ M_\odot$ at $Z = 10^{-4}$ and from $8.90 \pm 0.10\ M_\odot$ to $7.25 \pm 0.25\ M_\odot$ at $Z = 0.02$ (see Table 3 and Fig. 5). The magnitude of this effect is in good agreement with the recent study by Gil-Pons et al. (2007). Comparisons of our results with other computations including core overshooting (Bertelli et al. 1985; Castellani et al. 1985; Maeder & Meynet 1989; Girardi et al. 2000; Pols et al. 1998) show that C ignites at a higher initial mass in our models, implying a smaller core during the He burning phase. The reason for this discrepancy can be ascribed to the treatment of overshooting. Contrary to our diffusive approach, these authors (with the exception of Pols et al. 1998) used the "old recipe" in which instantaneous mixing is performed over a small region encompassing a fraction d of the pressure height scale at the core border ($d \times H_{\rm P}$). With $0.25 \leq d \leq 0.5$, this generates a much larger overshooting compared to that of our diffusive treatment with $f_{\rm over} = 0.016$[1], explaining why $M_{\rm up}$ is lower in their simulations.

In summary, the determination of $M_{\rm up}$ is highly dependent on the treatment of mixing at the edge of the convective He core. In this context, our values for $M_{\rm up}$ without overshooting must be considered as upper limits since diffusion was completely suppressed at the Schwarzschild boundary.

4.2. The mass transition M_{mass}

According to Nomoto (1984), if the ONe core mass ($M_{\rm ONe}$) at the end of the C-burning phase is greater than 1.37 $M_\odot$, the star proceeds through all nuclear burning stages and evolves into an iron core collapse SN. Following this definition, all our models having $M_{\rm ONe}$ above the horizontal solid line of Fig. 6 are tagged as "massive stars". $M_{\rm ONe}$ is defined as the mass coordinate of the

[1] The extent of the overshooting region obtained with a diffusive approach characterized by $f_{\rm over}$ corresponds approximately to what is expected using an instantaneous mixing approach with $d \simeq 10 \times f_{\rm over}$ (e.g. Herwig et al. 1997; Salasnich et al. 1999). Note also that the "∇ prescription" used by Pols et al. (1998) corresponds to a value of d that varies between 0.22 and 0.4 depending on the initial stellar mass.

Table 3. Transition masses and He core mass transitions as a function of initial metallicity Z. Y is the initial helium mass fraction, $M_{\rm n}$ is calculated without metallicity dependence in the mass loss rate for three different values of $\zeta = 35, 70, 350$ along with the corresponding He core mass ($M_{\rm up}^{\rm He}$). For each composition, we also indicate the values of $M_{\rm 2DUP}^{\rm He}$, $M_{\rm crit}^{\rm 2DUP}$ and $\zeta_{\rm crit}$

Z	Y	$M_{\rm ONe}$	$M_{\rm up}$	$M_{\rm up}^{\rm He}$	$M_{\rm n}$ $^{\zeta=35}$	$M_{\rm n}^{\rm He}$	$M_{\rm n}$ $^{\zeta=70}$	$M_{\rm n}^{\rm He}$	$M_{\rm n}$ $^{\zeta=350}$	$M_{\rm n}^{\rm He}$	$M_{\rm mas}$	$M_{\rm mas}^{\rm He}$	$M_{\rm 2DUP}$	$M_{\rm 2DUP}^{\rm He}$	$M_{\rm crit}^{\rm 2DUP}$	$\zeta_{\rm crit}$
10^{-5}	0.2479	1.04	7.60 ± 0.10	0.77	8.36	0.90	9.06	1.04	9.58	1.16	9.75	1.18	9.04	1.04	1.26	73
10^{-4}	0.2480	1.05	7.35 ± 0.15	0.76	8.28	0.93	9.02	1.03	9.53	1.15	9.66	1.18	9.03	1.03	1.28	88
0.001	0.2492	1.05	7.60 ± 0.10	0.77	8.37	0.92	9.06	1.05	9.63	1.15	9.78	1.18	9.04	1.05	1.26	71
0.004	0.2533	1.05	8.05 ± 0.05	0.78	8.75	0.93	9.48	1.05	10.13	1.14	10.26	1.18	9.53	1.06	1.28	93
0.008	0.2587	1.05	8.55 ± 0.05	0.81	9.39	0.89	9.99	1.04	10.52	1.15	10.66	1.18	10.04	1.06	1.27	81
0.02	0.2748	1.04	8.90 ± 0.10	0.78	9.65	0.90	10.44	1.04	10.83	1.15	10.93	1.18	10.54	1.06	1.26	82
0.04	0.3017	1.06	9.10 ± 0.10	0.80	9.65	0.90	10.20	1.04	10.77	1.15	10.89	1.18	10.53	1.10	1.29	106
10^{-4}	0.2480	1.08	5.85 ± 0.15	0.88	6.77	1.05	7.20	1.13	7.55	1.21	7.63	1.24	7.51	1.20	1.34	309
0.02	0.2748	1.11	7.25 ± 0.25	0.91	7.88	1.04	8.39	1.14	8.77	1.23	8.83	1.26	8.80	1.24	1.36	682

top of the C-burning layer where the nuclear energy production due to ^{12}C+^{12}C reactions has dropped below 10 erg g^{-1}cm^{-3}. Note that this definition is equivalent (to less than 0.01 $M_\odot$) to defining the core edge as the location e.g. where the ^{24}Mg abundance becomes larger than 10^{-3} in mass fraction. The end of the C-burning phase is defined as the time at which the peak temperature has decreased below 5.5×10^8 K and the carbon luminosity is less than 10 $L_\odot$ or just before neon ignites (i.e. when the neon luminosity in modulus is greater than 10^8 $L_\odot$ or is twice the carbon luminosity). This unusual definition of the end of C-burning was imposed by the fact that using central abundances would not have accounted for the secondary carbon flashes that develop after the flame has reached the center. The value of $M_{\rm mas}$ is then determined by interpolating in our grid of models the value of $M_{\rm ini}$ such that, at the end of the C-burning phase, $M_{\rm ONe}(M_{\rm mas}) = 1.37\ M_\odot$.

$M_{\rm mas}$ is directly connected to the core mass at the end of He burning and therefore shares the same properties: a minimum around $Z = 10^{-4}$ and a maximum around $Z = 0.04$ (Fig. 5). We also find that prior to C-ignition, little mass is lost by the star, thus making the determination of $M_{\rm mas}$ weakly dependent on the assumed mass loss rate prescription (Eq. (A.3)). Concerning the effects of overshooting, they are similar to those affecting $M_{\rm up}$ and the value of $M_{\rm mas}$ is globally decreased by $\sim$2 $M_\odot$, passing from 8.9–9.7 $M_\odot$ to 7.1–7.6 $M_\odot$ for $Z = 10^{-4}$ and from 10.3–10.9 $M_\odot$ to 8.3–8.9 $M_\odot$ for $Z = 0.02$ (see Table 3).

The minimum mass of our ONe WDs, deduced from Fig. 6, is of the order of $\sim$1.05–1.10 $M_\odot$ (Table 3), in agreement with the recent theoretical estimates of Gil-Pons et al. (2005). We note however that the minimum ONe WD mass is larger in our overshoot models, possibly because these stars develop more massive and thus hotter and less degenerate cores. Finally, let us emphasize that these numbers must be considered as lower limits since rotation, which would affect the size of the core, is not included in the simulations.

4.3. The mass transition M_n

The fate of SAGB stars depends on the evolution of the degenerate core mass after C-burning and whether or not it reaches the threshold value of $M_{\rm EC} \sim 1.37\ M_\odot$. If the envelope is expelled before this critical value is attained, the SAGB star ends its life as a ONe WD otherwise electron captures are activated and a supernovae explosion ensues. To determine the outcome of the evolution, we thus need to estimate the mass accreted onto the ONe core ($\Delta M_{\rm core}$) during the post C-burning phase.

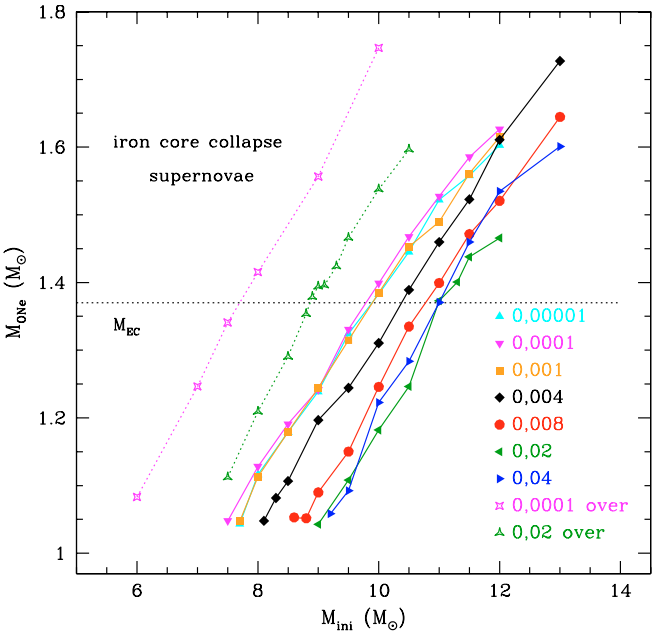

Fig. 6. Mass of the ONe core at the end of C-burning for the different initial compositions as a function of initial mass. Models with overshooting are connected by dotted lines. The horizontal line indicates the critical mass $M_{\rm EC} = 1.37\ M_\odot$ (see Sect. 4.2).

The rate of change on the envelope mass $\dot{M}_{\rm env}$ is given by

$$\dot{M}_{\rm env} = -\dot{M}_{\rm core} - \dot{M}_{\rm loss}. \quad (1)$$

where $\dot{M}_{\rm loss}$ ($\geq$0) and $\dot{M}_{\rm core}$ ($\geq$0) represent the mass loss and core growth rates, respectively. The post C-burning evolutionary timescale is given by $\tau_{\rm evol} = \min(\tau_{\rm core}, \tau_{\rm env})$ where $\tau_{\rm core}$ and $\tau_{\rm env}$ are defined by

$$\int_0^{\tau_{\rm core}} \dot{M}_{\rm core}\, {\rm d}t = M_{\rm EC} - M_{\rm core}^{\rm EAGB}, \quad (2)$$

$$\int_0^{\tau_{\rm env}} \dot{M}_{\rm env}\, {\rm d}t = -M_{\rm env}^{\rm EAGB}. \quad (3)$$

In these equations, the origin of times has been shifted to beginning of the SAGB phase, when the carbon burning luminosity $L_C < 10 L_\odot$ and the 2DUP is completed. At this time, the core and envelope masses are equal to $M_{\rm core}^{\rm EAGB}$ and $M_{\rm env}^{\rm EAGB}$, respectively and the stellar mass $M_{\rm EAGB}^{*} = M_{\rm core}^{\rm EAGB} + M_{\rm env}^{\rm EAGB}$. During

the post C-burning evolution, the mean values for $\dot{M}_{\rm core}$, $\dot{M}_{\rm env}$ and $\dot{M}_{\rm loss}$ are given by

$$\overline{\dot{M}}_{\rm core} = \frac{1}{\tau_{\rm evol}} \int_0^{\tau_{\rm evol}} \dot{M}_{\rm core}\, {\rm d}t,$$
$$\overline{\dot{M}}_{\rm env} = \frac{1}{\tau_{\rm evol}} \int_0^{\tau_{\rm evol}} \dot{M}_{\rm env}\, {\rm d}t,$$
$$\overline{\dot{M}}_{\rm loss} = \frac{1}{\tau_{\rm evol}} \int_0^{\tau_{\rm evol}} \dot{M}_{\rm loss}\, {\rm d}t.$$

For stars that avoid core collapse, $\tau_{\rm evol} = \tau_{\rm env} = \frac{-M_{\rm env}^{\rm EAGB}}{\overline{\dot{M}}_{\rm env}} < \tau_{\rm core}$, which in terms of the mean core growth rate translates into

$$\overline{\dot{M}}_{\rm core} < \frac{M_{\rm EC} - M_{\rm core}^{\rm EAGB}}{M_{\rm env}^{\rm EAGB} + M_{\rm core}^{\rm EAGB} - M_{\rm EC}} \overline{\dot{M}}_{\rm loss} \equiv \dot{M}_{\rm core}^{\rm crit}. \quad (4)$$

If this condition is satisfied, the maximum mass accreted onto the core before the envelope is lost is simply given by

$$\Delta M_{\rm core} = \overline{\dot{M}}_{\rm core} \times \tau_{\rm evol} = M_{\rm env}^{\rm EAGB} \frac{\overline{\dot{M}}_{\rm core}}{\overline{\dot{M}}_{\rm core} + \overline{\dot{M}}_{\rm loss}}. \quad (5)$$

It is important to note that in this approach $\Delta M_{\rm core}$ only depends on the initial envelope mass and on the ratio $\zeta = \frac{\overline{\dot{M}}_{\rm loss}}{\overline{\dot{M}}_{\rm core}} \geq 0$:

$$\Delta M_{\rm core} = \frac{M_{\rm env}^{\rm EAGB}}{1+\zeta}. \quad (6)$$

If the third dredge-up (3DUP) is present during the TP-SAGB phase with an efficiency[2] λ, the core growth rate is reduced and its effective value is then given by

$$\overline{\dot{M}}_{\rm core}(\lambda) = [1-\lambda] \times \overline{\dot{M}}_{\rm core}(\lambda = 0). \quad (7)$$

Typical core growth rates for SAGB stars can be found in the literature (Poelarends et al. 2006, 2007; Siess 2006b, 2007) and are of the order of $5 \times 10^{-7}\ M_\odot\,{\rm yr}^{-1}$.

Figure 7 illustrates the strong sensitivity of $\Delta M_{\rm core}$ to the different parameters (see also Poelarends et al. 2006, 2007). More quantitatively, for a characteristic envelope mass of $M_{\rm env}^{\rm EAGB} = 10\,M_\odot$ and a typical core growth rate of $\overline{\dot{M}}_{\rm core} = 5{\times}10^{-7}\ M_\odot\,{\rm yr}^{-1}$, we find that $\Delta M_{\rm core}$ varies between 0.02 and 0.16 $M_\odot$ as λ decreases from 0.9 to 0.3 if $\overline{\dot{M}}_{\rm loss} = 2 \times 10^{-5}\ M_\odot\,{\rm yr}^{-1}$. If we now allow the mass loss rate to vary between $10^{-4}\ M_\odot\,{\rm yr}^{-1}$ and $10^{-6}\ M_\odot\,{\rm yr}^{-1}$ for the given value of $\overline{\dot{M}}_{\rm core}$, we find that $0.05 \lesssim \Delta M_{\rm core}/M_\odot \lesssim 0.48$.

Determination of the final core mass proceeds as follows: the values of $M_{\rm core}^{\rm EAGB}$ and $M_{\rm env}^{\rm EAGB}$ are provided by our computed models then, for a given ζ, we calculate $M_{\rm core}^{\rm end} = M_{\rm core}^{\rm EAGB} + \Delta M_{\rm core}$ using Eq. (6). Finally, for each metallicity, the transition mass $M_{\rm n}$ is determined by interpolating in our database the value of $M_{\rm ini}$ such that $M_{\rm core}^{\rm end}(M_{\rm ini} = M_{\rm n}) = M_{\rm EC}$.

This approach is very simple and is far from reaching the level of sophistication of synthetic models (e.g. Marigo et al. 1996; Izzard et al. 2006). However, because our ultimate goal is to determine the endpoint of the evolution, such a refinement is not necessary. We do not intend to follow in this paper the detailed nucleosynthesis and structural evolution which would certainly require a more accurate description of the evolutionary properties of the SAGB star. Furthermore, we emphasize that no stellar models describing the full TP-SAGB phase are available yet, so even synthetic models would suffer large uncertainties in this mass range, especially concerning the free parameters λ, $\dot{M}_{\rm loss}$ and $M_{\rm core}^{\rm EAGB}$. Our approach minimizes the problem by hiding our "ignorance" in the parameter ζ and by skipping the details of the TP-SAGB evolution.

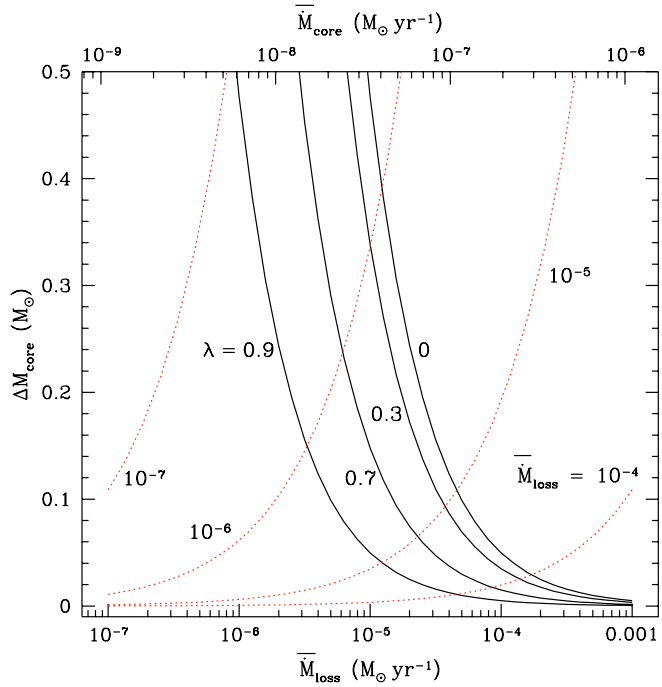

Fig. 7. Mass accreted on the ONe core ($\Delta M_{\rm core}$, Eq. (6)) as a function of the mass loss rate (solid lines, lower axis) for different values of the dredge-up parameter ($0 \leq \lambda \leq 0.9$ with $\overline{\dot{M}}_{\rm core} = 5 \times 10^{-7}\ M_\odot\,{\rm yr}^{-1}$) and as a function of the effective core growth rate (dotted lines, upper axis) for different values of the mass loss rate ranging between 10^{-4} and $10^{-7}\ M_\odot\,{\rm yr}^{-1}$. The envelope mass $M_{\rm env}^{\rm EAGB} = 10\,M_\odot$.

The value of $M_{\rm n}$ as a function of metallicity and ζ is presented in Fig. 8. Provided the dredge-up parameter λ remains less than one, $M_{\rm n}$ is confined to the mass range $M_{\rm up} < M_{\rm n} < M_{\rm mas}$. In the case of very strong mass loss or very efficient 3DUP (ζ very large), the amount of mass accreted onto the core is small. In these circumstances, only the most massive stars will enter the EC regime and $M_{\rm n}$ lies very close to $M_{\rm mas}$. Conversely, if $\overline{\dot{M}}_{\rm core}$ approaches $\dot{M}_{\rm core}^{\rm crit}$, even the least massive stars that ignite carbon (i.e. those with $M_{\rm ini} \simeq M_{\rm up}$) will be able to develop a core exceeding $M_{\rm EC}$ and in this case $M_{\rm n}$ approaches $M_{\rm up}$.

Without metallicity dependence in the mass loss rate, the $M_{\rm n}$ curves homothetically moves from $M_{\rm mas}$ to $M_{\rm up}$ as ζ decreases. We also note that a maximum is present around $Z = 0.02$. This latter feature results from the larger ONe core mass at the end of the C-burning phase for the He-rich $Z = 0.04$ models with $M_{\rm ini} \gtrsim 9.5\,M_\odot$ (Fig. 1). If now a scaling factor $\sqrt{Z/Z_\odot}$ (Kudritzki et al. 1987) is applied to $\overline{\dot{M}}_{\rm loss}$, the shape of the curves changes as illustrated in the top panel of Fig. 8. We emphasize that this treatment of the metallicity dependence is not accurate because during the TP-SAGB phase the surface composition changes as a result of hot bottom burning and/or 3DUP episodes. However even with this limitation, this model illustrates the important point that at lower metallicities, because of the reduced

[2] By definition $\lambda = \frac{\Delta M_{\rm dredge}}{\Delta M_{\rm H}}$ is the ratio between the amount of mass dredged-up by the convective envelope $\Delta M_{\rm dredge}$ by the amount by which the core mass has increased during the preceding interpulse period $\Delta M_{\rm H}$, respectively.

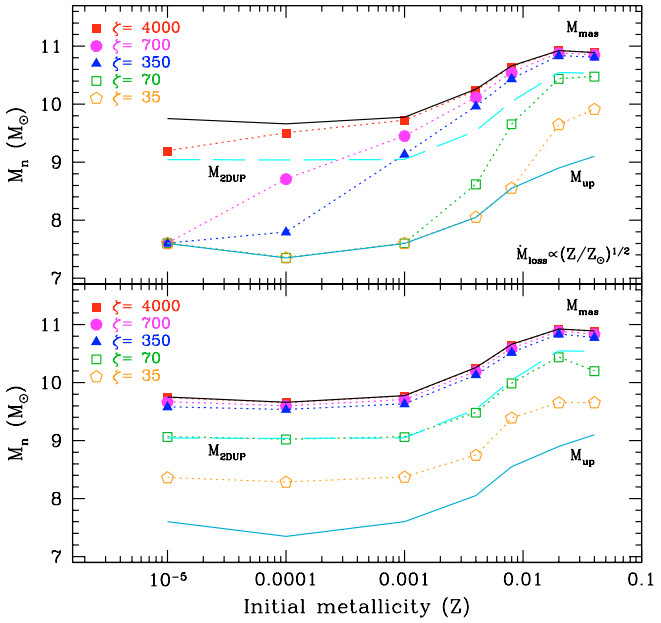

Fig. 8. The behavior of $M_{\rm n}$ (solid lines with symbols) for our models without overshooting as function of initial metallicity and ζ. $M_{\rm up}$ and $M_{\rm mas}$ are also shown (lower and upper long-dashed lines, respectively). Below $M_{\rm up}$, evolution leads to the formation of a CO WD, between $M_{\rm up}$ and $M_{\rm n}$ the outcome is the formation of a ONe WD, above $M_{\rm n}$, the evolutionary endpoint is the formation of a neutron star and for $M_{\rm ini} > M_{\rm mas}$ the star evolves through all nuclear burning stages up to iron core collapse SN. The short-dashed line represents the value of $M_{\rm 2DUP}$ above which the second dredge-up does not take place. As seen in Sect. 5, stars with $M_{\rm n} > M_{\rm 2DUP}$ avoid the EC-SN channel. In the upper panel, a metallicity dependence of $\sqrt{Z/Z_\odot}$ has been applied to the mass loss rate in the determination of $M_{\rm n}$.

mass loss rate efficiency (Bowen & Willson 1991), more mass can accumulate on top of the core. The formation rate of ONe WDs is thus considerably reduced and restricted to a narrower mass range: for a given ζ the region between $M_{\rm up}$ and $M_{\rm n}$ decreases with Z. A corollary of this implication is that the supernova rate must have been larger in the past as a consequence of additional contributions from EC-SN (see also Gil-Pons et al. 2007 and Poelarends et al. 2007).

Trying to estimate ζ is a difficult task. Given the high temperature of the HBS in SAGB stars ($>10^8$ K, Siess 2007), the typical interpulse core growth rate is of the order of $\sim 5 \times 10^{-7}\ M_\odot\,{\rm yr}^{-1}$. This value depends however on the ability of the convective envelope to penetrate into the CO rich region of the thermal pulse during the 3DUP. In the abundant literature on AGB stars (Herwig 2005), the characteristics of 3DUP (time of occurrence, depth, long term evolution) are still debated and are sensitive to numerical factors such as spatial resolution (Straniero et al. 1997), interpolation of constitutive variables (Pols & Tout 2001), definition of the convective boundaries (Frost & Lattanzio 1996) or to the method used for solving the stellar structure equations (Stancliffe 2006), but also to the physical mixing processes acting at the base of the convective envelope (rotational mixing, gravity waves or overshooting). For λ in the interval [0, 0.9] (see Karakas et al. 2002 for a study of the dependence of λ on Z and $M_{\rm ini}$ in lower mass AGB stars), we can estimate that $5 \times 10^{-8} \lesssim \dot{\overline{M}}_{\rm core}/(M_\odot\,{\rm yr}^{-1}) \lesssim 5 \times 10^{-7}$.

The mass loss rate is also affected by large uncertainties and depends on many parameters such as chemical composition or extra mixing. The case of SAGB stars is particularly ambiguous because no specific mass loss prescription is available, reasonable values range between the usual rates for intermediate and massive stars. For a typical SAGB star of $\sim 10^5\ L_\odot$, $\sim 1200\ R_\odot$ and $T_{\rm eff} \simeq 3000$ K, the Vassiliadis & Wood (1993) prescription gives $\dot{M} \simeq 1.5 \times 10^{-4}\ M_\odot\,{\rm yr}^{-1}$ while the Blöcker (1995) formulation leads to $8.5 \times 10^{-3}\ M_\odot\,{\rm yr}^{-1}$ and the de Jager (1988) prescription for massive stars to $5.3 \times 10^{-6}\ M_\odot\,{\rm yr}^{-1}$. These estimates illustrate the large range of plausible values, which may be further affected if rotation and/or metallicity dependence are accounted for. In addition, these numbers represent instantaneous rates which may not correspond to the average values we are looking for. Estimates of $\dot{\overline{M}}_{\rm env} = M_{\rm env}^{\rm EAGB}/\tau_{\rm evol}$ based on the models of Karakas (2003) indicate that in the mass range $\sim$6–6.5 $M_\odot$, $\dot{\overline{M}}_{\rm env} \simeq 5 \times 10^{-6}$–$10^{-5}\ M_\odot\,{\rm yr}^{-1}$ with a clear tendency for $\dot{\overline{M}}_{\rm env}$ to increase with $M_{\rm ini}$. So we may consider $5 \times 10^{-6}\ M_\odot\,{\rm yr}^{-1}$ as a reasonable lower estimate for SAGB stars. For the higher possible value of $\dot{\overline{M}}_{\rm env}$ we hypothetically assume $10^{-4}\ M_\odot\,{\rm yr}^{-1}$.

With these numbers, ζ varies between a few tens to almost 10^5 when λ is very small. For a "realistic" choice of the parameters ($\lambda \approx$ [0.3–0.9], $\dot{\overline{M}}_{\rm core} \approx 5 \times 10^{-7}\ M_\odot\,{\rm yr}^{-1}$ and $\dot{\overline{M}}_{\rm env} \approx 5 \times 10^{-4}\ M_\odot\,{\rm yr}^{-1}$) we get $\zeta \simeq$ [35–100]. From Fig. 8 and assuming no metallicity dependence in $\dot{\overline{M}}_{\rm env}$ (lower panel), we find that the supernova-channel for SAGB stars (the area between $M_{\rm n}$ and $M_{\rm mas}$) is limited to a narrow mass range of $\sim$1–1.5 $M_\odot$ width at most. It may concern stars with initial masses ranging between 8–9 $M_\odot$ at very low Z and up to 9.5–11 $M_\odot$ at solar metallicity. If a scaling factor is applied to the mass-loss rate in the calculation of $M_{\rm n}$, the occurrence of EC-SN is strongly enhanced and below $Z \lesssim 10^{-3}$, the formation of ONe WDs appears very difficult through the single stellar evolution channel.

Finally, as for $M_{\rm up}$ and $M_{\rm mas}$, the consideration of core overshooting in the computations leads to a downward shift of all the masses by $\sim 2\ M_\odot$. In this case, solar metallicity stars of $\sim 7\ M_\odot$ could evolve to EC-SN.

5. The impact of the second dredge-up

As well as bringing nuclearly processed material to the surface, the 2DUP also contributes to mixing hydrogen inward. As such, it has the ability to hamper an eventual core collapse by reducing the H-exhausted core mass below a critical value $M_{\rm crit}^{\rm 2DUP}$ close to the Chandrasekhar mass limit ($M_{\rm Ch}$). In practice, $M_{\rm crit}^{\rm 2DUP}$ is determined by extrapolating linearly the low values of the H-depleted core mass ($M_{\rm H-free}^{\rm 2DUP} < M_{\rm EC}$ in Fig. 9) at the mass coordinate corresponding to the intersection of the $M_{\rm H-free}^{\rm 2DUP}$ curves with $M_{\rm EC}$. Our simulations indicate that $M_{\rm crit}^{\rm 2DUP} \simeq 1.28 \pm 0.01\ M_\odot$ and $1.35 \pm 0.01\ M_\odot$ for the models without and with overshooting, respectively (Table 3).

As displayed in Fig. 9, for each set of models, the H-exhausted core mass steadily increases with $M_{\rm ini}$ and abruptly jumps above $\sim$2.4–2.6 $M_\odot$ as it approaches $M_{\rm crit}^{\rm 2DUP}$. In all cases, the jump occurs in a narrow mass interval of $\lesssim 0.5\ M_\odot$ width, marking a clear transition to core collapse structures (Podsiadlowski et al. 2004). For decreasing metallicities and/or if overshooting is taken into account, the star develops a more massive core and the 2DUP occurs at a lower initial mass. The initial mass where this transition occurs is referred to as $M_{\rm 2DUP}$ and is determined by linearly interpolating our data at the point where $M_{\rm H-free}^{\rm 2DUP}(M_{\rm 2DUP}) = M_{\rm crit}^{\rm 2DUP}$. As for $M_{\rm mas}$, the value of $M_{\rm 2DUP}$ is weakly dependent on the mass loss rate. We also note the increasing reduction of the H-depleted core mass ($\Delta M_{\rm 2DUP}$) as $M_{\rm ini}$ approaches $M_{\rm 2DUP}$.

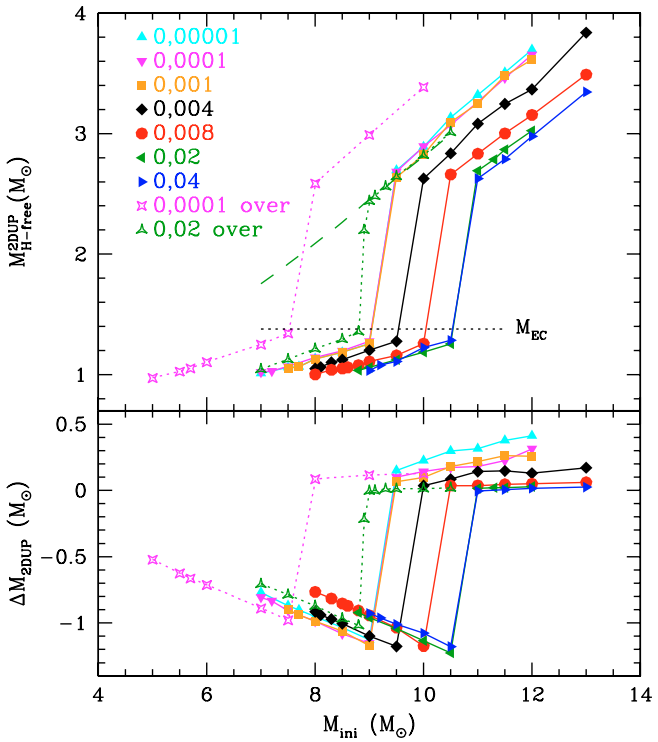

Fig. 9. (*Top*) mass of the H-exhausted core after completion of the 2DUP (M^{2DUP}_{H-free} is defined as the coordinate of the bottom of the convective envelope at its deepest extent during the 2DUP) for the different metallicities as a function of the initial stellar mass. The models with overshooting are connected by dotted lines. The horizontal dotted lines represent the Chandrasekhar mass limit. For the $Z = 0.02$ models with overshooting, the dashed line represents the location of the HBS at the end of core He burning, prior to the second dredge-up. (*Bottom*) mass extent of the convective envelope into the H-depleted core during the 2DUP. ΔM_{2DUP} corresponds to the difference between the mass coordinate of the top of the HBS estimated before and after the completion of the 2DUP. Only the models with $M_{ini} < M_{2DUP}$ ($\Delta M_{2DUP} < 0$) suffer a reduction of their H-depleted cores.

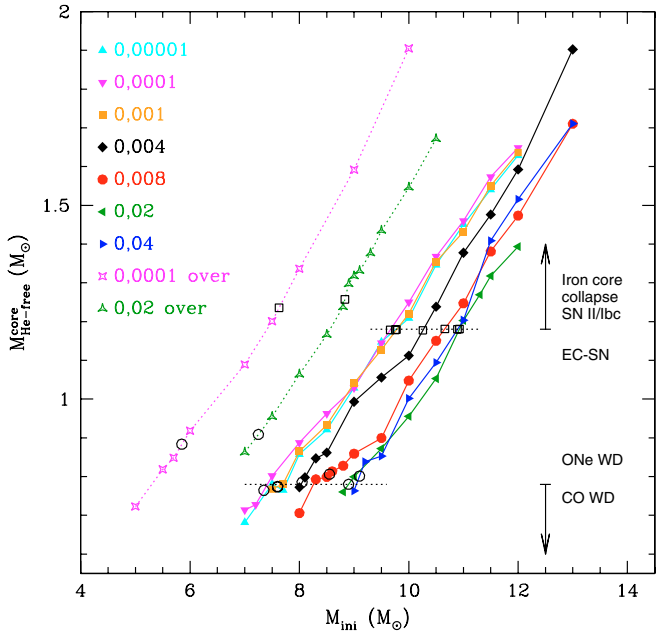

Fig. 10. Mass of the CO core ($M^{core}_{He-free}$) at the end of central He burning for the different metallicities as a function of M_{ini}. $M^{core}_{He-free}$ is defined as the mass coordinate of the locus of maximum nuclear energy production due to He burning when the central He mass fraction has dropped below 10^{-4}. The large open circles (squares) represent M^{He}_{up} (M^{He}_{mas}, see Sect. 5) and the dotted horizontal lines roughly indicate the critical He core masses above which the nature of remnant and of the outcome change.

Considering that stars with $M_{ini} > M_{2DUP}$ will not enter the TP-SAGB phase but instead pursue their evolution through advanced nuclear-burning stages, we can deduce some constraints on the parameter ζ which defines M_n. According to this assumption, a necessary condition for a star to avoid iron core collapse can be stated as $M_n < M_{2DUP}$ which, after some algebra (see Appendix B for details), translates into $\zeta < \zeta_{crit}$ where ζ_{crit} satisfies $M_n(\zeta_{crit}) = M_{2DUP}$.

If no metallicity dependence of the mass loss rate is considered, our models indicate that ζ_{crit} is weakly dependent on the initial stellar composition, varying between ~70 and 90 for our considered metallicities (Table 3). This result teaches us that if during the post C-burning phase the ratio of $\overline{M}_{env}$ to $\overline{M}_{core}$ is larger than ~70−90 (and if we discard a metallicity dependence on the mass loss rate), stars with $M_{ini} \geq M_n$ will never evolve into an EC-SN because in the absence of 2DUP the H depleted core remains more massive than M_{EC} and the evolution proceeds, as for massive stars, up to iron core collapse. Stated otherwise, the evolutionary path leading to EC-SN can only be accessible if $\zeta \lesssim 70-90$ or equivalently if $M_n < M_{ini} < M_{2DUP}$. Note that in this context the definition of M_{mas} should be revised to take into account the effect of the 2DUP and in practice should be set to $M_{mas} = M_{2DUP}$. For typical values of $\overline{M}_{core}$ in the range 5×10^{-8} to 5×10^{-7} $M_\odot$ yr^{-1}, the evolution to EC-SN requires that $\overline{M}_{loss} \gtrsim 5 \times 10^{-5}-5 \times 10^{-6}$ $M_\odot$ yr^{-1} for stars with $M_{ini} > M_n$. Such mass loss rates can be easily achieved by standard AGB prescriptions, provided they still hold for higher mass stars. Considering that realistic values for ζ are in the range [35−100] as estimated before, we see that the mass window for EC-SN (the region in Fig. 8 between $35 \lesssim \zeta \lesssim 100$) is relatively narrow and approximately constant in this case, of the order of ~0.7−0.8 $M_\odot$. Using a more sophisticated and independent approach, Poelarends et al. (2007) came to the same conclusion: the mass window for EC-SNe varies dramatically with the dredge-up efficiency and mass loss rate, i.e. on ζ and using their solar metallicity models, it ranges between 0.2−1.4 $M_\odot$. The small mass range for which a star can evolve to EC-SN strengthens the argument developed by Podsiadlowski et al. (2004) that binarity might provide a better channel for this evolutionary path.

If we now account for an explicit dependence of the mass loss rate on Z, according to Eq. (B.4) the value of ζ_{crit} increases as the metallicity drops. For example, at $Z = 10^{-4}$, $\zeta \lesssim 700-900$. According to our criterion and if we adopt the same estimates for $\overline{M}_{core}$ as before, lower metallicity stars need to develop stronger winds than their solar metallicity counterpart to avoid the EC-SN. This is at odds with the generally accepted idea that mass loss rate efficiency decreases with metallicity. Therefore, as pointed out by Gil-Pons et al. (2007), the rate of EC-SN must have been larger in the past.

6. The critical He core mass M^{He}_{up}, M^{He}_{mas} and M^{He}_{n}

In this section, we investigate how these different transition masses are connected to the core properties during He burning. We have estimated from the data provided in Fig. 10, the

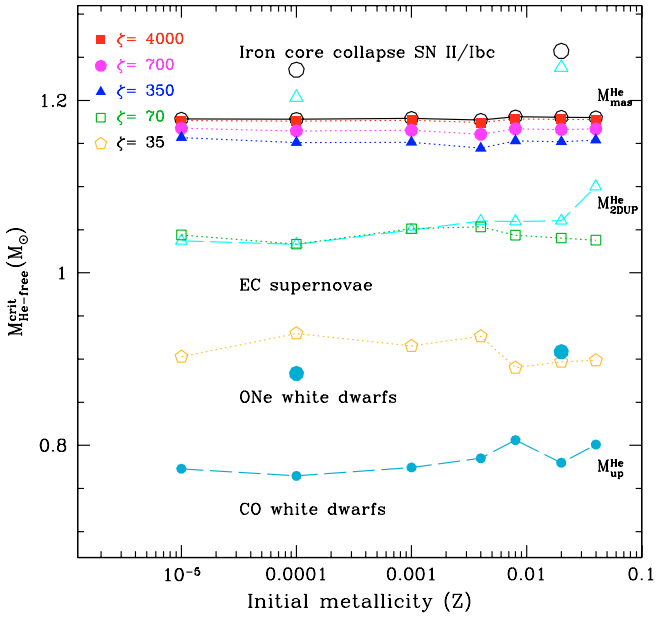

Fig. 11. CO core mass at the end of core He burning corresponding to the models with initial mass equal to $M_{\rm up}$ (dashed, filled dots), $M_{\rm mas}$ (solid, open circles), $M_{\rm n}$ (dotted lines, filled squares) and $M^{\rm He}_{\rm 2DUP}$ (dashed, open triangles) as a function of metallicity. From top to bottom, the different dotted lines correspond to decreasing values of ζ from 4000 to 35 as in Fig. 8.

CO core mass ($M^{\rm core}_{\rm He-free}$) corresponding to the models with initial masses equal to $M_{\rm up}$, $M_{\rm mas}$ and $M_{\rm n}$. These values are referred to as $M^{\rm He}_{\rm up}$, $M^{\rm He}_{\rm mas}$ and $M^{\rm He}_{\rm n}$, respectively and their dependence on metallicity is displayed in Fig. 11.

Our models indicate that the critical CO core mass is weakly dependent on the initial composition. Stars with $M_{\rm ini} = M_{\rm up}$ have on average $M^{\rm He}_{\rm up}$ equal to $\sim 0.783 \pm 0.015\ M_\odot$ and $\sim 0.896 \pm 0.018\ M_\odot$ for the models without and with overshooting, respectively. The difference of $\sim 0.1\ M_\odot$ between these values is related to the fact that, for a given core size, the models without overshooting have a larger initial mass. Therefore, at helium exhaustion, they contract more efficiently, releasing additional heat which facilitates carbon ignition. Concerning the critical core mass above which an iron core forms, we find that $M^{\rm He}_{\rm mas} \simeq 1.179 \pm 0.001\ M_\odot$ and $M^{\rm He}_{\rm mas} \simeq 1.246 \pm 0.015\ M_\odot$ for models without and with overshooting, respectively. Depending on the prescriptions for the mass loss and core growth rates (i.e. according to ζ), the value of $M^{\rm He}_{\rm n}$ can in principle cover the entire range between $M^{\rm He}_{\rm up}$ and $M^{\rm He}_{\rm mas}$, which represents a mass interval of $\sim 0.2\ M_\odot$. Note that these critical He core masses are not affected by the 2DUP which skims the top of HeBS later in the evolution. $M^{\rm He}_{\rm 2DUP}$ is relatively constant below $Z = Z_\odot$ with a mean value of $1.050 \simeq \pm 0.012$ and rises at high metallicity, as a consequence of the initially higher He content in these models (Fig. 1).

In summary, if at the end of He burning, the CO core mass is less than $\simeq 0.8\ M_\odot$, the (single) star will never ignite carbon, if it exceeds $\simeq 1.05\ M_\odot$ the 2DUP will not occur and if it larger than $\simeq 1.25\ M_\odot$, the evolution will proceed through all the nuclear burning stages. As confirmed by this study (see Pols et al. 1998), for a given treatment of convective mixing, these limiting CO core masses are almost independent of the initial composition.

7. Summary and final comments

We present new results of extensive computations of SAGB models up to the end of C-burning covering a large range of initial masses and metallicities and accounting for the presence of core overshooting. All the data are available at `http://www-astro.ulb.ac.be/~siess/database.html` with the hope they can be useful for synthetic computations.

Analysis of the data indicates that prior to C-burning the evolutionary properties of the SAGB stars are very similar to those of lower mass stars and in particular the chemical signatures of the 1DUP are basically identical. The evolution starts to diverge at C-ignition. Carbon burning proceeds the usual way: a flash followed by the propagation of a deflagration front to the center. Less massive stars develop more degenerate cores and ignite carbon at larger radii through more energetic C-flashes. After the passage of the flame, some unburnt ^{12}C can be preserved in the core but significant traces (mass fraction $\gtrsim 0.015$) are only present in the least massive models which are not thought to follow EC-SN. The main observational difference between SAGB and intermediate mass stars is probably the strong He enrichment that follows the second dredge-up. In our models, this enrichment can be as large as 40–50% reaching $Y \simeq 0.26$–0.40, clearly identifying SAGB as potentially strong contributors to the galactic helium production.

Our models also enable us to determine several mass transitions and to analyze their dependence on metallicity, mass loss and core growth rates. The transition masses $M_{\rm up}$, $M_{\rm n}$ and $M_{\rm mas}$ present a nonlinear behavior with Z characterized by a minimum around $Z = 10^{-4}$ which is connected to opacity effects and to the higher efficiency of the pp-chains at lower metallicities. These values are extremely sensitive to the treatment of mixing at the convective boundaries. When core overshooting is taken into account, the values of $M_{\rm up}$, $M_{\rm n}$ and $M_{\rm mas}$ are lowered by $\sim 2\ M_\odot$. We also outline the insidious numerical effects associated with the modeling of central He burning which can strongly affect the size of the convective core.

The fraction of SAGB stars that evolve into the WD or neutron star channel depends critically on the interplay between mass loss and core growth. The large uncertainties associated with these parameters prevent a precise estimate of the initial mass range that leads to EC-SNe which appears to be restricted to a very narrow mass interval of typically less than $\sim 1\ M_\odot$ in width. We show that the existence of a supernova channel for SAGB stars is intimately connected to the second dredge-up phenomenon. Using this evolutionary link, we have been able to infer some constraints on the parameters defining the final fate of SAGB stars. In particular, we have determined that the ratio of the mean mass loss rate to the mean core growth rate during the post C-burning phase ζ ($=\overline{\dot{M}}_{\rm loss}/\overline{\dot{M}}_{\rm core}$) must be less than ~ 70–90 for EC-SN to occur because, for higher values of ζ, the second dredge-up is avoided and the star evolves as a massive star through iron core collapse SN.

The minimum mass for an ONe WD derived from our models is about $1.05\ M_\odot$. This is in agreement with the recent simulations of Gil-Pons et al. (2005) of primordial SAGBs and with the indirect determination of Wanajo et al. (1999) who constrained the WD mass by fitting the nucleosynthesis signature of ONe novae with observations.

The evolution of SAGB stars is particularly sensitive to the physical assumptions and numerics. It is thus highly encouraged that additional computations of models in this mass range be made, both to explore the parameter space and also to gauge the uncertainties associated with the use of different stellar evolution

codes. Ultimately these models will enable quantification of the role of SAGB stars in the chemical evolution of galaxies.

Acknowledgements. M. L. Pumo participated in the analysis of the stellar models. This paper and in particular Sect. 3 benefited from her input. The author warmly thanks the anonymous referee for his/her constructive comments that improved the presentation of the results. I am also very grateful to R. G. Izzard for his comments and careful reading of the manuscript.

Appendix A: Analytical fits

In this appendix, based on our large set of computed models we provide analytical fits to several quantities including core masses and dredge-up depths as a function of mass and initial composition. From Figs. 6, 9 and 10 the relations between the different masses and the initial model mass $M_{\rm ini}$ are quite linear and, to a good approximation, may be approximated by

$$M = \alpha + \beta\, M_{\rm ini} \tag{A.1}$$

where the coefficients α and β depend on the initial helium content Y and metallicity (Z) and are derived using a Levenberg-Marquardt iterative χ^2-minimization method (Press et al. 1992). The derived formulae have a relative accuracy $\delta := \Delta M/M < 4\%$ and an absolute error of at most $\Delta := \Delta M < 0.1\, M_\odot$. The relations presented below do not include the overshoot models.

The ONe core mass at the beginning of the SAGB phase $M^*_{\rm ONe}$ is given by

$$M^*_{\rm ONe} = a + bM_{\rm ini} \tag{A.2}$$

where

$$\begin{aligned} a =\ & -0.325 + -4.745\log(Y/Y_\odot) + 0.351\log(Z/Z_\odot) \\ & +3.291\log(Y/Y_\odot)\log(Z/Z_\odot) \\ b =\ & 0.151 + 0.237\log(Y/Y_\odot) - 0.0166\log(Z/Z_\odot) \\ & -0.156\log(Y/Y_\odot)\log(Z/Z_\odot). \end{aligned}$$

For this fit, $\Delta \lesssim 0.06\, M_\odot$ and $\delta < 4\%$.

At the end of carbon burning, the stellar mass can be accurately approximated by

$$M^*_{\rm EAGB} = c + dM_{\rm ini} \tag{A.3}$$

where

$$\begin{aligned} c =\ & -0.322 - 5.378\log(Y/Y_\odot) + 0.9125\log(Z/Z_\odot) \\ & +8.577\log(Y/Y_\odot)\log(Z/Z_\odot) \\ d =\ & 1.002 + 0.218\log(Y/Y_\odot) - 0.0753\log(Z/Z_\odot) \\ & -0.706\log(Y/Y_\odot)\log(Z/Z_\odot). \end{aligned}$$

The maximum relative error $\delta \lesssim 1\%$ and $\Delta < 0.01\, M_\odot$.

For stars which suffer a reduction of their core mass during the 2DUP, i.e. those with ($M^{\rm 2DUP}_{\rm H-free} < M^{\rm 2DUP}_{\rm crit}$), the mass coordinate of the bottom of the convective envelope after the completion of the 2DUP is given by

$$M^{\rm 2DUP\downarrow}_{\rm core} = e + fM_{\rm ini} \tag{A.4}$$

where

$$\begin{aligned} e =\ & -0.222 - 2.563\log(Y/Y_\odot) - 7.867\times10^{-4}\log(Z/Z_\odot) \\ & +0.0701\log(Y/Y_\odot)\log(Z/Z_\odot) \\ f =\ & 0.141 - 0.005\log(Y/Y_\odot) + 0.0208\log(Z/Z_\odot) \\ & +0.186\log(Y/Y_\odot)\log(Z/Z_\odot) \end{aligned}$$

with $\Delta < 0.04\, M_\odot$ and $\delta < 3\%$ while for the massive stars that avoid the 2DUP ($M^{\rm 2DUP}_{\rm H-free} > 2.3$)

$$M^{\rm 2DUP\uparrow}_{\rm core} = g + hM_{\rm ini} \tag{A.5}$$

where

$$\begin{aligned} g =\ & -0.898 + 3.509\log(Y/Y_\odot) - 0.528\log(Z/Z_\odot) \\ & -4.922\log(Y/Y_\odot)\log(Z/Z_\odot) \\ h =\ & 0.323 - 0.909\log(Y/Y_\odot) + 0.0887\log(Z/Z_\odot) \\ & +0.839\log(Y/Y_\odot)\log(Z/Z_\odot) \end{aligned}$$

($\Delta < 0.08\, M_\odot$, $\delta < 3\%$).

The relation between $M_{\rm 2DUP}$ and $M^{\rm core}_{\rm He-free}$, the maximum extent of the core He burning zone, is almost independent of the initial composition since this dependence is already included in $M^{\rm core}_{\rm He-free}$. For stars undergoing efficient 2DUP, to a very good approximation ($\Delta < 0.03\, M_\odot$, $\delta < 3\%$), we have

$$M^{\rm 2DUP\downarrow}_{\rm core} = 0.4661 + 0.7598 M^{\rm core}_{\rm He-free}. \tag{A.6}$$

We also report a strong correlation, almost independent of the composition, between $M^{\rm core}_{\rm He-free}$ and $M^*_{\rm ONe}$

$$M^*_{\rm ONe} = 0.2061 + 1.2519\, M^{\rm core}_{\rm He-free} - 0.2406(M^{\rm core}_{\rm He-free})^2 \tag{A.7}$$

with $\Delta < 0.04\, M_\odot$ and $\delta < 3\%$.

Using the same interpolation formula as Iben & Becker (1979), we derived (from Table 3) the following fits for $M_{\rm up}$ ($\Delta < 0.067\, M_\odot$), $M_{\rm 2DUP}$ ($\Delta < 0.020\, M_\odot$) and $M_{\rm mas}$ ($\Delta < 0.021\, M_\odot$):

$$\begin{aligned} M_{\rm up} =\ & 8.904 + 22.325\log(Y/Y_\odot) + 72.612\log(Y/Y_\odot)^2 \\ & -1.881\log(Z/Z_\odot) + 0.017\log(Z/Z_\odot)^2 \\ & -19.259\log(Y/Y_\odot)\log(Z/Z_\odot) \end{aligned} \tag{A.8}$$

$$\begin{aligned} M_{\rm 2DUP} =\ & 10.917 + 35.982\log(Y/Y_\odot) + 112.729\log(Y/Y_\odot)^2 \\ & -3.482\log(Z/Z_\odot) - 0.020\log(Z/Z_\odot)^2 \\ & -30.577\log(Y/Y_\odot)\log(Z/Z_\odot) \end{aligned} \tag{A.9}$$

$$\begin{aligned} M_{\rm mas} =\ & 10.522 + 47.514\log(Y/Y_\odot) + 102.887\log(Y/Y_\odot)^2 \\ & -4.369\log(Z/Z_\odot) - 0.050\log(Z/Z_\odot)^2 \\ & -35.744\log(Y/Y_\odot)\log(Z/Z_\odot). \end{aligned} \tag{A.10}$$

Appendix B: Derivation of $\zeta_{\rm crit}$

By definition of $M_{\rm n}$, the final core mass $M^{\rm end}_{\rm core}(M_{\rm n}) = M_{\rm EC} = M^{\rm 2DUP}_{\rm H-free}(M_{\rm n}) + \Delta M_{\rm core}(M_{\rm n})$ which, using Eq. (6), reads

$$\zeta M^{\rm 2DUP}_{\rm H-free}(M_{\rm n}) + M^*_{\rm n} = (1+\zeta)M_{\rm EC}. \tag{B.1}$$

In this equation, $M^*_{\rm n} = M^*(M_{\rm n})$ is given by Eq. (A.3). Now injecting Eqs. (A.3) and (A.4) into (B.1) we find an expression for $M_{\rm n}$ that depends only on ζ (and initial composition)

$$M_{\rm n} = \frac{(1+\zeta)M_{\rm EC} - c - e\zeta}{d + f\zeta}\cdot \tag{B.2}$$

As stated in Sect. 5, a necessary condition for a star to avoid iron core collapse can be formulated by $M_{\rm n} < M_{\rm 2DUP}$. Using Eq. (A.4) and the fact that by definition $M^{\rm 2DUP\downarrow}_{\rm core}(M_{\rm 2DUP}) = M^{\rm 2DUP}_{\rm crit}$, we find that the condition finally writes

$$\zeta < \zeta_{\rm crit} = \frac{(M^{\rm 2DUP}_{\rm crit} - e)\, d + f(c - M_{\rm EC})}{f(M_{\rm EC} - M^{\rm 2DUP}_{\rm crit})}\cdot \tag{B.3}$$

$\zeta_{\rm crit}$ is a function of the initial stellar composition (though the variables c, d, e, f) and of $M^{\rm 2DUP}_{\rm crit}$ only. If a metallicity dependence on $\dot{M}_{\rm loss}$ is accounted for, then ζ must satisfy

$$\zeta < \zeta_{\rm crit}\left(\frac{Z}{Z_\odot}\right)^{-1/2}\cdot \tag{B.4}$$

Appendix C: Database of stellar models

All the stellar models presented in this work can be found at and downloaded from: `http://www-astro.ulb.ac.be/~siess/database.html`. For each model star, two files are available: the *.hrd* files gather "observational" properties including the evolutionary path of the star in the HR diagram, the mass loss rate, photospheric quantities and the evolution of the surface mass fractions of the main elements up to ^{26}Mg. The *.struc* files compile information about the evolution of structural quantities including the nuclear luminosities (dues to H, He, neutrinos), the central density and temperature, the central chemical composition, the mass coordinate of the convective core and convective envelope, the temperature at the base of the envelope and the location of the H and He burning shells. An interactive graphic tool is also available at `http://www-astro.ulb.ac.be/~siess/server/sagb_plot.html` and allows the user to plot the different variables. Data from different star models can be compared this way.

In addition, the two tables (Tables 4 and 5) presenting the surface composition at the end of the first and second dredge-up and only available in the electronic version of this paper can also be retreived from the author's web site.

References

Arnould, M., Goriely, S., & Jorissen, A. 1999, A&A, 347, 572
Blöcker, T. 1995, A&A, 297, 727
Blöcker, T., Holweger, H., Freytag, B., et al. 1998, Space Sci. Rev., 85, 105
Becker, S. A., & Iben, I. 1979, ApJ, 232, 831
Becker, S. A., & Iben, I. 1980, ApJ, 237, 111
Bertelli, G., Bressan, A. G., & Chiosi, C. 1985, A&A, 150, 33
Bono, G., Caputo, F., Cassisi, S., et al. 2000, ApJ, 543, 955
Bowen, G. H., & Willson, L. A. 1991, ApJ, 375, L53
Charbonnel, C. 2006, EAS Publ. Ser., 19, 125
Cappellaro, E., Riello, M., Altavilla, G., et al. 2005, A&A, 430, 83
Cassisi, S., & Castellani, V. 1993, ApJS, 88, 509
Castellani, V., Chieffi, A., Pulone, L., & Tornambè, A. 1985, ApJ, 294, L31
Chieffi, A., & Tornambè, A. 1986, MNRAS, 220, 529
Chiosi, C., Bertelli, G., & Bressan, A. 1992, ARA&A, 30, 235
Chugai, N. N., & Utrobin, V. P. 2000, A&A, 354, 557
Coc, A., Vangioni-Flam, E., Descouvemont, P., Adahchour, A., & Angulo, C. 2004, ApJ, 600, 544
Costa, V., Pumo, M. L., Bonanno, A., & Zappalà, R. A. 2006, A&A, 447, 641
de Jager, C., Nieuwenhuijzen, H., & van der Hucht, K. A. 1988, A&AS, 72, 259
Dessart, L., Burrows, A., Ott, C. D., et al. 2003, ApJ, 644, 1063
Doherty, C. L., & Lattanzio, J. C. 2006, MmSAI, 77, 828
Dominguez, I., Straniero, O., Tornambé, A., & Isern, J. 1996, ApJ, 472, 783
Dominguez, I., Chieffi, A., Limongi, M., & Straniero, O. 1999, ApJ, 524, 226
Eldridge, J. J., & Tout, C. A. 2004, MNRAS, 353, 87
Ferrario, L., Wickramasinghe, D., Liebert, J., & Williams, K. A. 2005, A&A, 361, 1131
Finley, D. S., Koester, D., & Basri, G. 1997, ApJ, 488, 375
Freytag, B., Ludwig, H.-G., & Steffen, M. 1996, A&A, 313, 497
Frost, C. A., & Lattanzio, J. C. 1996, ApJ, 473, 383
García-Berro, E., & Iben, I. 1994, ApJ, 434, 306
García-Berro, E., Ritossa, C., & Iben, I. 1997, ApJ, 485, 765
Gil-Pons, P., & García-Berro, E. 2002, A&A, 396, 589
Gil-Pons, P., García-Berro, E., José, J., Hernanz, M., & Truran, J. W. 2003, A&A, 407, 1021
Gil-Pons, P., Suda, T., Fujimoto, M. Y., & García-Berro, E. 2005, A&A, 433, 1037
Gil-Pons, P., Gutiérrez, J., & García-Berro, E. 2007, A&A, 464, 667
Girardi, L., Bressan, A., Bertilli, G., & Chiosi, C. 2000, A&AS, 141, 371
Grevesse, N., Noels, A., & Sauval, A. J. 1996, ASPC, 99, 117
Guerrero, J., Garía-Berro, E., & Isern, J. 2004, A&A, 413, 257
Gutiérrez, J., García-Berro, E., Iben, I., et al. 1996, ApJ, 459, 701
Gutiérrez, J., Canal, R., & García-Berro, E. 2005, A&A, 435, 231
Hendry, M. A., Smartt, S. J., Maund, J. R., et al. 2005, MNRAS, 359, 906
Hendry, M. A., Smartt, S. J., Crockett, R. M., et al. 2006, MNRAS, 369, 1303
Herwig, F. 2005, ARA&A, 43, 435
Herwig, F., Blöcker, T., Schoenberner, D., & El Eid, M. 1997, A&A, 324, L81
Hillebrandt, W. 1982, A&A, 110, L3
Hillebrandt, W., Nomoto, K., & Wolff, R. G. 1984, A&A, 133, 175
Iben, I., Ritossa, C., & García-Berro, E. 1997, ApJ, 489, 772
Imbriani, G., Limongi, M., Gialanella, L., Straniero, O., & Chieffi, A. 2001, ApJ, 558, 903
Izzard, R. G., Dray, L. M., Karakas, A. I., et al. 2006, A&A, 460, 565
José, J., & Hernanz, M. 1998, ApJ, 494, 680
José, J., Coc, A., & Hernanz, M. 2001, ApJ, 560, 897
Karakas, A. I. 2003, Ph.D. Thesis (Monash University)
Karakas, A. I., Lattanzio, J. C., & Pols, O. R. 2002, PASA, 19, 515
Kitaura, F. S., Janka, H.-Th., & Hillebrandt, W. 2006, A&A, 450, 345
Kudritzki, R. P., Pauldrach, A., & Puls, J. 1987, A&A, 173, 293
Li, W., Wang, X., Van Dyk, S. D., et al. 2007, ApJ, 661, 1013
Liebert, J., Bergeron, P., & Holberg, J. B. 2005, ApJS, 156, L47
Maeder, A., & Meynet, G. 1989, A&A, 210, 155
Marigo, P., Bressan, A., & Chiosi, C. 1996, A&A, 313, 545
Marsh, M. C., Barstow, M. A., Buckley, D. A., et al. 1997, MNRAS, 286, 369
Maund, J. R., Smartt, S. J., & Danziger, I. J. 2005, MNRAS, 364, L33
Miyaji, S., Nomoto, K., Yokoi, K., & Sugimoto, D. 1980, Publ. Astron. Soc. Japan, 32, 303
Miyaji, S., & Nomoto, K. 1987, ApJ, 318, 307
Nomoto, K. 1981, IAU Symp., 93, 295
Nomoto, K. 1984, ApJ, 277, 791
Nomoto, K., Sugimoto, D., Sparks, W. M., et al. 1983, Nature, 299, 803
Podsiadlowski, Ph., Langer, N., Poelarends, A. J. T., et al. 2004, ApJ, 612, 1044
Poelarends, A. J. T., Izzard, R. G., Herwig, F., et al. 2006, MmSAI, 77, 846
Poelarends, A. J. T., Herwig, F., Langer, N., & Heger, A. 2007, ApJ, in press
Pols, O. R., & Tout, C. A. 2001, MemSaIt, 72, 299
Pols, O. R., Schroder, K.-P., Hurley, J. R., et al. 1998, MNRAS, 298, 525
Press, W. K., Teukolsky, S. A., Vetterling, W. T., & Flannery, B. P. 1992, Numerical recipes in FORTRAN (Cambridge University press)
Ratnatunga, K. U., & Van Den Bergh, S. 1989, ApJ, 343, 713
Reimers, D. 1975, Problems in stellar atmospheres and Envelopes, ed. B. Baschek, W. H. Kegel, & G. Traving (Berlin Heidelberg New York: Springer-Verlag)
Ritossa, C., García-Berro, E., & Iben, I. 1996, ApJ, 460, 489
Ritossa, C., García-Berro, E., & Iben, I. 1999, ApJ, 515, 381
Salasnich, B., Bressan, A., & Chiosi, C. 1999, A&A, 342, 131
Schaller, G., Schaerer, D., Meynet, G., & Maeder, A. 1992, A&AS, 96, 269
Segretain, L., Chabrier, G., & Mochkovitch, R. 1997, ApJ, 481, 355
Siess, L. 2006a, A&A, 448, 717 (Paper I)
Siess, L. 2006b, EAS Publications Series, 19, 103
Siess, L. 2007, Why galaxies care about AGB stars, ed. F. Kerschbaum, C. Charbonnel, & B. Wing, ASP Conf. Ser., in press
Siess, L., & Pumo, M. L. 2006c, MmSAI, 77, 822
Stancliffe, R. 2006, MNRAS, 370, 1817
Straniero, O., Chieffi, A., Limongi, M., et al. 1997, ApJ, 478, 332.
Straniero, O., Dominguez, I., Imbriani, G., & Piersanti, L. 2003, ApJ, 583, 878
Sumiyoshi, K., Terasawa, M., Mathews, G. J., et al. 2001, ApJ, 562, 880
Timmes, F. X., Woosley, S. E., & Taam, R. E. 1994, ApJ, 420, 348
Tornambè, A., & Chieffi, A. 1986, MNRAS, 220, 529
Umeda, H., Nomoto, K., Yamaoka, H., & Wanajo, S. 1999, ApJ, 513, 861
Vassiliadis, E., & Wood, P. R. 1993, ApJ, 413, 641
Vennes, S. 1999, ApJ, 525, 995
Wanajo, S., Tamamura, M., Itoh, N., et al. 2003, ApJ, 593, 968
Wanajo, S., Hashimoto, M., & Nomoto, K. 1999, ApJ, 523, 409
Webbink, R. F. 1990, in The Physics of Classical Novae, ed. A. Cassatella, & R. Viotti (Berlin: Springer), Proc. IAU Coll., 122, 405
Weidemann, V. 2000, A&A, 363, 647
Woosley, S. E., Heger, A., & Weaver, T. A. 2002, Rev. Mod. Phys., 74, 1015
Zampieri, L., Pastorello, A., Turatto, M., et al. 2003, MNRAS, 338, 711

Online Material

Table 4. Envelope mass fraction of selected species at the end of the 1DUP.

$M_{\rm ini}$	^{1}H	^{3}He	^{4}He	^{12}C	^{13}C	^{14}N	^{15}N	^{16}O	^{17}O	^{18}O	^{21}Ne	^{22}Ne	^{23}Na	^{25}Mg	^{26}Mg
	Z = 0.00001														
7.0	0.7520	3.696(–5)	0.2479	1.703(–6)	2.214(–8)	5.237(–7)	8.879(–9)	4.784(–6)	3.906(–9)	1.082(–8)	7.012(–9)	7.332(–8)	1.791(–8)	2.942(–8)	5.538(–8)
7.5	0.7520	3.697(–5)	0.2479	1.703(–6)	2.206(–8)	5.238(–7)	8.568(–9)	4.784(–6)	3.862(–9)	1.082(–8)	6.814(–9)	7.325(–8)	1.796(–8)	2.978(–8)	5.491(–8)
7.7	0.7520	3.697(–5)	0.2479	1.703(–6)	2.208(–8)	5.237(–7)	8.637(–9)	4.784(–6)	3.875(–9)	1.082(–8)	6.864(–9)	7.327(–8)	1.795(–8)	2.969(–8)	5.503(–8)
8.0	0.7520	3.697(–5)	0.2479	1.703(–6)	2.207(–8)	5.238(–7)	8.597(–9)	4.784(–6)	3.871(–9)	1.082(–8)	6.842(–9)	7.326(–8)	1.796(–8)	2.973(–8)	5.498(–8)
8.5	0.7520	3.697(–5)	0.2479	1.703(–6)	2.206(–8)	5.238(–7)	8.555(–9)	4.784(–6)	3.867(–9)	1.082(–8)	6.820(–9)	7.325(–8)	1.796(–8)	2.977(–8)	5.493(–8)
9.0	0.7520	3.697(–5)	0.2479	1.703(–6)	2.205(–8)	5.238(–7)	8.478(–9)	4.784(–6)	3.859(–9)	1.082(–8)	6.776(–9)	7.324(–8)	1.798(–8)	2.984(–8)	5.482(–8)
9.5	0.7520	3.696(–5)	0.2479	1.703(–6)	2.207(–8)	5.238(–7)	8.530(–9)	4.784(–6)	3.875(–9)	1.082(–8)	6.835(–9)	7.325(–8)	1.796(–8)	2.974(–8)	5.496(–8)
10.0	0.7520	3.696(–5)	0.2479	1.703(–6)	2.210(–8)	5.238(–7)	8.643(–9)	4.784(–6)	3.891(–9)	1.082(–8)	6.903(–9)	7.327(–8)	1.794(–8)	2.961(–8)	5.513(–8)
10.5	0.7520	3.696(–5)	0.2479	1.703(–6)	2.213(–8)	5.237(–7)	8.748(–9)	4.784(–6)	3.912(–9)	1.082(–8)	6.984(–9)	7.329(–8)	1.792(–8)	2.946(–8)	5.532(–8)
11.0	0.7520	3.695(–5)	0.2479	1.703(–6)	2.213(–8)	5.237(–7)	8.739(–9)	4.784(–6)	3.913(–9)	1.082(–8)	6.985(–9)	7.329(–8)	1.792(–8)	2.946(–8)	5.532(–8)
11.5	0.7520	3.695(–5)	0.2479	1.703(–6)	2.216(–8)	5.237(–7)	8.845(–9)	4.784(–6)	3.932(–9)	1.082(–8)	7.062(–9)	7.331(–8)	1.790(–8)	2.932(–8)	5.550(–8)
12.0	0.7520	3.695(–5)	0.2479	1.703(–6)	2.217(–8)	5.237(–7)	8.889(–9)	4.784(–6)	3.942(–9)	1.082(–8)	7.103(–9)	7.332(–8)	1.789(–8)	2.925(–8)	5.560(–8)
	Z = 0.0001														
7.0	0.7518	1.019(–4)	0.2480	1.703(–5)	2.153(–7)	5.246(–6)	6.405(–8)	4.786(–5)	3.421(–8)	1.082(–7)	5.368(–8)	7.297(–7)	1.831(–7)	3.245(–7)	5.145(–7)
7.2	0.7518	1.019(–4)	0.2480	1.703(–5)	2.151(–7)	5.246(–6)	6.362(–8)	4.786(–5)	3.412(–8)	1.082(–7)	5.338(–8)	7.297(–7)	1.832(–7)	3.251(–7)	5.138(–7)
7.5	0.7518	1.019(–4)	0.2480	1.703(–5)	2.152(–7)	5.246(–6)	6.381(–8)	4.786(–5)	3.418(–8)	1.082(–7)	5.355(–8)	7.297(–7)	1.832(–7)	3.248(–7)	5.142(–7)
8.0	0.7518	1.019(–4)	0.2480	1.703(–5)	2.152(–7)	5.246(–6)	6.358(–8)	4.786(–5)	3.415(–8)	1.082(–7)	5.342(–8)	7.297(–7)	1.832(–7)	3.250(–7)	5.139(–7)
8.5	0.7518	1.018(–4)	0.2480	1.703(–5)	2.152(–7)	5.246(–6)	6.370(–8)	4.786(–5)	3.420(–8)	1.082(–7)	5.353(–8)	7.297(–7)	1.832(–7)	3.248(–7)	5.142(–7)
9.0	0.7518	1.018(–4)	0.2480	1.703(–5)	2.152(–7)	5.246(–6)	6.381(–8)	4.786(–5)	3.425(–8)	1.082(–7)	5.364(–8)	7.297(–7)	1.832(–7)	3.246(–7)	5.144(–7)
9.5	0.7518	1.018(–4)	0.2480	1.703(–5)	2.153(–7)	5.246(–6)	6.401(–8)	4.786(–5)	3.432(–8)	1.082(–7)	5.382(–8)	7.297(–7)	1.831(–7)	3.242(–7)	5.149(–7)
10.0	0.7518	1.018(–4)	0.2480	1.703(–5)	2.154(–7)	5.246(–6)	6.448(–8)	4.786(–5)	3.445(–8)	1.082(–7)	5.419(–8)	7.297(–7)	1.830(–7)	3.235(–7)	5.158(–7)
10.5	0.7518	1.018(–4)	0.2480	1.703(–5)	2.156(–7)	5.246(–6)	6.497(–8)	4.786(–5)	3.459(–8)	1.082(–7)	5.457(–8)	7.298(–7)	1.830(–7)	3.228(–7)	5.167(–7)
11.0	0.7518	1.018(–4)	0.2480	1.703(–5)	2.157(–7)	5.245(–6)	6.545(–8)	4.786(–5)	3.472(–8)	1.082(–7)	5.495(–8)	7.299(–7)	1.829(–7)	3.221(–7)	5.176(–7)
11.5	0.7518	1.017(–4)	0.2480	1.703(–5)	2.158(–7)	5.245(–6)	6.592(–8)	4.786(–5)	3.485(–8)	1.082(–7)	5.532(–8)	7.299(–7)	1.828(–7)	3.214(–7)	5.185(–7)
12.0	0.7518	1.017(–4)	0.2480	1.703(–5)	2.160(–7)	5.245(–6)	6.637(–8)	4.786(–5)	3.497(–8)	1.082(–7)	5.567(–8)	7.300(–7)	1.827(–7)	3.207(–7)	5.193(–7)
	Z = 0.001														
10.0	0.7497	1.016(–4)	0.2492	1.704(–4)	2.061(–6)	5.266(–5)	2.498(–7)	4.789(–4)	2.131(–7)	1.082(–6)	2.612(–7)	7.278(–6)	1.894(–6)	3.776(–6)	4.475(–6)
10.5	0.7497	1.016(–4)	0.2492	1.704(–4)	2.061(–6)	5.266(–5)	2.504(–7)	4.789(–4)	2.134(–7)	1.082(–6)	2.617(–7)	7.278(–6)	1.894(–6)	3.775(–6)	4.476(–6)
11.0	0.7497	1.016(–4)	0.2492	1.704(–4)	2.061(–6)	5.266(–5)	2.510(–7)	4.789(–4)	2.137(–7)	1.082(–6)	2.622(–7)	7.278(–6)	1.894(–6)	3.774(–6)	4.478(–6)
11.5	0.7497	1.016(–4)	0.2492	1.704(–4)	2.062(–6)	5.266(–5)	2.517(–7)	4.789(–4)	2.140(–7)	1.082(–6)	2.627(–7)	7.278(–6)	1.894(–6)	3.773(–6)	4.479(–6)
12.0	0.7497	1.015(–4)	0.2492	1.704(–4)	2.062(–6)	5.266(–5)	2.522(–7)	4.789(–4)	2.142(–7)	1.082(–6)	2.631(–7)	7.278(–6)	1.894(–6)	3.772(–6)	4.480(–6)
7.5	0.7497	1.017(–4)	0.2492	1.704(–4)	2.060(–6)	5.267(–5)	2.464(–7)	4.789(–4)	2.116(–7)	1.082(–6)	2.588(–7)	7.278(–6)	1.895(–6)	3.781(–6)	4.469(–6)
7.7	0.7497	1.017(–4)	0.2492	1.704(–4)	2.060(–6)	5.266(–5)	2.467(–7)	4.789(–4)	2.118(–7)	1.082(–6)	2.590(–7)	7.278(–6)	1.895(–6)	3.780(–6)	4.470(–6)
8.0	0.7497	1.017(–4)	0.2492	1.704(–4)	2.061(–6)	5.266(–5)	2.472(–7)	4.789(–4)	2.120(–7)	1.082(–6)	2.593(–7)	7.278(–6)	1.895(–6)	3.780(–6)	4.471(–6)
8.5	0.7497	1.017(–4)	0.2492	1.704(–4)	2.061(–6)	5.266(–5)	2.478(–7)	4.789(–4)	2.123(–7)	1.082(–6)	2.598(–7)	7.278(–6)	1.895(–6)	3.779(–6)	4.472(–6)
9.0	0.7497	1.017(–4)	0.2492	1.704(–4)	2.061(–6)	5.266(–5)	2.485(–7)	4.789(–4)	2.125(–7)	1.082(–6)	2.603(–7)	7.278(–6)	1.894(–6)	3.778(–6)	4.473(–6)
9.5	0.7497	1.016(–4)	0.2492	1.704(–4)	2.061(–6)	5.266(–5)	2.492(–7)	4.789(–4)	2.128(–7)	1.082(–6)	2.608(–7)	7.278(–6)	1.894(–6)	3.777(–6)	4.474(–6)
	Z = 0.004														
8.0	0.7425	6.824(–5)	0.2535	4.406(–4)	2.285(–5)	4.777(–4)	4.012(–7)	1.914(–3)	2.738(–6)	3.177(–6)	9.521(–7)	2.759(–5)	9.187(–6)	1.529(–5)	1.767(–5)
8.1	0.7425	6.777(–5)	0.2534	4.403(–4)	2.287(–5)	4.779(–4)	4.007(–7)	1.914(–3)	2.753(–6)	3.174(–6)	9.523(–7)	2.758(–5)	9.197(–6)	1.529(–5)	1.767(–5)
8.3	0.7425	6.651(–5)	0.2534	4.372(–4)	2.277(–5)	4.817(–4)	3.976(–7)	1.914(–3)	2.988(–6)	3.150(–6)	9.527(–7)	2.744(–5)	9.343(–6)	1.529(–5)	1.767(–5)
8.5	0.7425	6.553(–5)	0.2534	4.356(–4)	2.274(–5)	4.839(–4)	3.958(–7)	1.913(–3)	3.139(–6)	3.136(–6)	9.531(–7)	2.736(–5)	9.435(–6)	1.529(–5)	1.767(–5)
9.0	0.7421	6.287(–5)	0.2537	4.286(–4)	2.253(–5)	5.021(–4)	3.891(–7)	1.902(–3)	3.613(–6)	3.080(–6)	9.657(–7)	2.697(–5)	9.839(–6)	1.524(–5)	1.772(–5)
9.5	0.7418	6.077(–5)	0.2541	4.234(–4)	2.240(–5)	5.198(–4)	3.840(–7)	1.888(–3)	3.918(–6)	3.037(–6)	9.804(–7)	2.663(–5)	1.019(–5)	1.519(–5)	1.777(–5)
10.5	0.7304	5.505(–5)	0.2655	3.994(–4)	2.164(–5)	6.521(–4)	3.655(–7)	1.770(–3)	3.632(–6)	2.848(–6)	1.357(–6)	2.498(–5)	1.185(–5)	1.439(–5)	1.860(–5)
10.0	0.7404	5.859(–5)	0.2555	4.165(–4)	2.221(–5)	5.569(–4)	3.782(–7)	1.855(–3)	3.808(–6)	2.982(–6)	1.036(–6)	2.618(–5)	1.064(–5)	1.502(–5)	1.795(–5)
11.5	0.7290	5.341(–5)	0.2670	3.989(–4)	2.177(–5)	6.541(–4)	3.632(–7)	1.769(–3)	3.597(–6)	2.838(–6)	1.382(–6)	2.489(–5)	1.202(–5)	1.437(–5)	1.862(–5)
11.0	0.7328	5.448(–5)	0.2631	4.011(–4)	2.177(–5)	6.412(–4)	3.656(–7)	1.780(–3)	3.722(–6)	2.858(–6)	1.286(–6)	2.505(–5)	1.181(–5)	1.450(–5)	1.849(–5)
12.0	0.7210	5.167(–5)	0.2750	3.939(–4)	2.237(–5)	6.923(–4)	3.539(–7)	1.732(–3)	2.584(–6)	2.805(–6)	1.581(–6)	2.467(–5)	1.233(–5)	1.401(–5)	1.898(–5)
13.0	0.7379	5.906(–5)	0.2581	4.583(–4)	2.498(–5)	5.001(–4)	4.041(–7)	1.863(–3)	1.807(–6)	3.268(–6)	1.112(–6)	2.750(–5)	9.289(–6)	1.493(–5)	1.805(–5)
	Z = 0.008														
8.0	0.7292	6.453(–5)	0.2626	8.451(–4)	4.337(–5)	1.125(–3)	7.650(–7)	3.683(–3)	7.950(–6)	6.056(–6)	2.001(–6)	5.174(–5)	2.192(–5)	3.021(–5)	3.571(–5)
8.3	0.7289	6.359(–5)	0.2630	8.441(–4)	4.349(–5)	1.135(–3)	7.643(–7)	3.673(–3)	6.816(–6)	6.038(–6)	2.015(–6)	5.200(–5)	2.165(–5)	3.016(–5)	3.576(–5)
8.5	0.7283	6.250(–5)	0.2635	8.388(–4)	4.332(–5)	1.157(–3)	7.583(–7)	3.656(–3)	6.745(–6)	5.997(–6)	2.036(–6)	5.175(–5)	2.190(–5)	3.009(–5)	3.583(–5)
8.6	0.7281	6.209(–5)	0.2638	8.383(–4)	4.379(–5)	1.159(–3)	7.551(–7)	3.654(–3)	6.588(–6)	6.007(–6)	2.044(–6)	5.182(–5)	2.183(–5)	3.007(–5)	3.586(–5)
8.8	0.7277	6.185(–5)	0.2641	8.429(–4)	4.318(–5)	1.163(–3)	7.632(–7)	3.644(–3)	6.497(–6)	6.013(–6)	2.059(–6)	5.170(–5)	2.195(–5)	3.002(–5)	3.591(–5)
9.0	0.7269	6.017(–5)	0.2650	8.325(–4)	4.333(–5)	1.190(–3)	7.507(–7)	3.626(–3)	7.432(–6)	5.944(–6)	2.089(–6)	5.096(–5)	2.271(–5)	2.993(–5)	3.600(–5)
9.5	0.7260	5.860(–5)	0.2659	8.290(–4)	4.341(–5)	1.214(–3)	7.458(–7)	3.604(–3)	7.169(–6)	5.909(–6)	2.127(–6)	5.070(–5)	2.299(–5)	2.981(–5)	3.613(–5)
10.0	0.7231	5.681(–5)	0.2688	8.199(–4)	4.327(–5)	1.266(–3)	7.372(–7)	3.557(–3)	6.955(–6)	5.833(–6)	2.231(–6)	5.008(–5)	2.360(–5)	2.951(–5)	3.643(–5)
10.5	0.7211	5.561(–5)	0.2707	8.165(–4)	4.334(–5)	1.292(–3)	7.327(–7)	3.532(–3)	6.578(–6)	5.800(–6)	2.306(–6)	4.986(–5)	2.382(–5)	2.931(–5)	3.664(–5)
11.0	0.7119	5.336(–5)	0.2800	7.979(–4)	4.289(–5)	1.413(–3)	7.185(–7)	3.420(–3)	5.978(–6)	5.650(–6)	2.624(–6)	4.836(–5)	2.532(–5)	2.855(–5)	3.743(–5)
11.5	0.7047	5.163(–5)	0.2872	7.840(–4)	4.256(–5)	1.487(–3)	7.065(–7)	3.355(–3)	5.635(–6)	5.537(–6)	2.871(–6)	4.744(–5)	2.626(–5)	2.801(–5)	3.799(–5)
12.0	0.6997	5.049(–5)	0.2922	7.765(–4)	4.249(–5)	1.531(–3)	6.994(–7)	3.314(–3)	5.219(–6)	5.474(–6)	3.043(–6)	4.676(–5)	2.699(–5)	2.765(–5)	3.835(–5)
13.0	0.6933	4.861(–5)	0.2987	7.679(–4)	4.268(–5)	1.601(–3)	6.893(–7)	3.247(–3)	4.577(–6)	5.391(–6)	3.269(–6)	4.573(–5)	2.812(–5)	2.711(–5)	3.890(–5)
	Z = 0.02														
8.8	0.6868	5.893(–5)	0.2930	2.100(–3)	1.070(–4)	3.138(–3)	1.889(–6)	8.858(–3)	1.525(–5)	1.490(–5)	5.236(–6)	1.253(–4)	5.893(–5)	7.470(–5)	9.011(–5)
9.0	0.6864	5.834(–5)	0.2934	2.098(–3)	1.072(–4)	3.155(–3)	1.885(–6)	8.842(–3)	1.508(–5)	1.487(–5)	5.258(–6)	1.250(–4)	5.920(–5)	7.462(–5)	9.020(–5)
9.5	0.6855	5.700(–5)	0.2943	2.092(–3)	1.075(–4)	3.187(–3)	1.873(–6)	8.813(–3)	1.449(–5)	1.481(–5)	5.308(–6)	1.247(–4)	5.949(–5)	7.443(–5)	9.039(–5)
10.0	0.6845	5.585(–5)	0.2953	2.086(–3)	1.077(–4)	3.226(–3)	1.863(–6)	8.777(–3)	1.399(–5)	1.475(–5)	5.364(–6)	1.243(–4)	5.999(–5)	7.422(–5)	9.061(–5)
10.5	0.6840	5.492(–5)	0.2958	2.084(–3)	1.081(–4)	3.248(–3)	1.855(–6)	8.754(–3)	1.357(–5)	1.471(–5)	5.405(–6)	1.239(–4)	6.033(–5)	7.406(–5)	9.078(–5)
11.0	0.6833	5.408(–5)	0.2965	2.081(–3)	1.085(–4)	3.274(–3)	1.846(–6)	8.730(–3)	1.310(–5)	1.467(–5)	5.451(–6)	1.237(–4)	6.060(–5)	7.389(–5)	9.096(–5)
11.3	0.6823	5.357(–5)	0.2975	2.077(–3)	1.086(–4)	3.307(–3)	1.840(–6)	8.697(–3)	1.286(–5)	1.463(–5)	5.500(–6)	1.232(–4)	6.114(–5)	7.371(–5)	9.114(–5)
11.5	0.6819	5.327(–5)	0.2979	2.075(–3)	1.088(–4)	3.321(–3)	1.837(–6)	8.683(–3)	1.268(–5)	1.462(–5)	5.524(–6)	1.229(–4)	6.138(–5)	7.362(–5)	9.123(–5)

Table 4. continued.

$M_{\rm ini}$	^{1}H	^{3}He	^{4}He	^{12}C	^{13}C	^{14}N	^{15}N	^{16}O	^{17}O	^{18}O	^{21}Ne	^{22}Ne	^{23}Na	^{25}Mg	^{26}Mg
12.0	0.6760	5.205(–5)	0.3039	2.052(–3)	1.086(–4)	3.456(–3)	1.815(–6)	8.562(–3)	1.185(–5)	1.442(–5)	5.754(–6)	1.214(–4)	6.295(–5)	7.290(–5)	9.197(–5)
	$Z = 0.04$														
9.0	0.6362	5.649(–5)	0.3235	4.323(–3)	2.167(–4)	5.930(–3)	3.861(–6)	1.794(–2)	3.056(–5)	3.050(–5)	1.002(–5)	2.513(–4)	1.173(–4)	1.508(–4)	1.788(–4)
9.2	0.6364	5.638(–5)	0.3233	4.345(–3)	2.185(–4)	5.829(–3)	3.863(–6)	1.802(–2)	3.576(–5)	3.067(–5)	1.000(–5)	2.525(–4)	1.161(–4)	1.509(–4)	1.787(–4)
9.5	0.6352	5.539(–5)	0.3245	4.312(–3)	2.173(–4)	5.997(–3)	3.837(–6)	1.788(–2)	2.984(–5)	3.038(–5)	1.008(–5)	2.498(–4)	1.189(–4)	1.505(–4)	1.791(–4)
10.0	0.6346	5.448(–5)	0.3251	4.304(–3)	2.180(–4)	6.032(–3)	3.817(–6)	1.785(–2)	2.812(–5)	3.029(–5)	1.013(–5)	2.501(–4)	1.185(–4)	1.503(–4)	1.793(–4)
10.5	0.6340	5.372(–5)	0.3257	4.300(–3)	2.189(–4)	6.080(–3)	3.800(–6)	1.781(–2)	2.756(–5)	3.022(–5)	1.018(–5)	2.488(–4)	1.199(–4)	1.501(–4)	1.795(–4)
11.0	0.6331	5.300(–5)	0.3266	4.293(–3)	2.196(–4)	6.128(–3)	3.783(–6)	1.776(–2)	2.644(–5)	3.014(–5)	1.024(–5)	2.483(–4)	1.204(–4)	1.498(–4)	1.798(–4)
11.5	0.6327	5.247(–5)	0.3270	4.293(–3)	2.206(–4)	6.152(–3)	3.770(–6)	1.773(–2)	2.546(–5)	3.011(–5)	1.028(–5)	2.481(–4)	1.207(–4)	1.496(–4)	1.800(–4)
12.0	0.6316	5.189(–5)	0.3281	4.292(–3)	2.219(–4)	6.212(–3)	3.757(–6)	1.766(–2)	2.498(–5)	3.007(–5)	1.036(–5)	2.464(–4)	1.224(–4)	1.493(–4)	1.803(–4)
13.0	0.6295	5.089(–5)	0.3302	4.283(–3)	2.232(–4)	6.316(–3)	3.728(–6)	1.756(–2)	2.338(–5)	2.993(–5)	1.050(–5)	2.449(–4)	1.240(–4)	1.488(–4)	1.809(–4)
	overshooting $Z = 0.0001$														
5.0	0.7518	1.020(–4)	0.2480	1.703(–5)	2.158(–7)	5.246(–6)	6.570(–8)	4.786(–5)	3.461(–8)	1.082(–7)	5.509(–8)	7.300(–7)	1.828(–7)	3.219(–7)	5.179(–7)
5.5	0.7518	1.020(–4)	0.2480	1.703(–5)	2.163(–7)	5.245(–6)	6.802(–8)	4.786(–5)	3.499(–8)	1.082(–7)	5.637(–8)	7.303(–7)	1.825(–7)	3.196(–7)	5.209(–7)
5.7	0.7518	1.020(–4)	0.2480	1.703(–5)	2.161(–7)	5.245(–6)	6.726(–8)	4.786(–5)	3.483(–8)	1.082(–7)	5.585(–8)	7.302(–7)	1.826(–7)	3.205(–7)	5.197(–7)
6.0	0.7518	1.020(–4)	0.2480	1.703(–5)	2.157(–7)	5.245(–6)	6.568(–8)	4.786(–5)	3.451(–8)	1.082(–7)	5.478(–8)	7.300(–7)	1.829(–7)	3.225(–7)	5.172(–7)
7.0	0.7518	1.019(–4)	0.2480	1.703(–5)	2.153(–7)	5.246(–6)	6.404(–8)	4.786(–5)	3.423(–8)	1.082(–7)	5.372(–8)	7.297(–7)	1.831(–7)	3.244(–7)	5.146(–7)
7.5	0.7518	1.019(–4)	0.2480	1.703(–5)	2.152(–7)	5.246(–6)	6.367(–8)	4.786(–5)	3.417(–8)	1.082(–7)	5.351(–8)	7.297(–7)	1.832(–7)	3.248(–7)	5.141(–7)
8.0	0.7518	1.019(–4)	0.2480	1.703(–5)	2.151(–7)	5.246(–6)	6.344(–8)	4.786(–5)	3.414(–8)	1.082(–7)	5.337(–8)	7.296(–7)	1.832(–7)	3.251(–7)	5.138(–7)
9.0	0.7518	1.018(–4)	0.2480	1.703(–5)	2.152(–7)	5.246(–6)	6.365(–8)	4.786(–5)	3.425(–8)	1.082(–7)	5.362(–8)	7.297(–7)	1.832(–7)	3.246(–7)	5.144(–7)
10.0	0.7518	1.018(–4)	0.2480	1.703(–5)	2.153(–7)	5.246(–6)	6.365(–8)	4.786(–5)	3.432(–8)	1.082(–7)	5.373(–8)	7.297(–7)	1.831(–7)	3.244(–7)	5.147(–7)
	overshooting $Z = 0.02$														
7.0	0.6786	6.946(–5)	0.3013	2.187(–3)	1.088(–4)	3.148(–3)	1.997(–6)	8.729(–3)	1.540(–5)	1.563(–5)	5.360(–6)	1.249(–4)	5.914(–5)	7.454(–5)	9.028(–5)
7.5	0.6793	6.679(–5)	0.3006	2.187(–3)	1.089(–4)	3.149(–3)	1.989(–6)	8.728(–3)	1.444(–5)	1.559(–5)	5.379(–6)	1.250(–4)	5.913(–5)	7.442(–5)	9.040(–5)
8.0	0.6790	6.470(–5)	0.3008	2.196(–3)	1.106(–4)	3.145(–3)	1.986(–6)	8.719(–3)	1.388(–5)	1.563(–5)	5.420(–6)	1.248(–4)	5.936(–5)	7.426(–5)	9.057(–5)
8.5	0.6790	6.278(–5)	0.3008	2.189(–3)	1.100(–4)	3.162(–3)	1.980(–6)	8.710(–3)	1.317(–5)	1.555(–5)	5.453(–6)	1.246(–4)	5.949(–5)	7.412(–5)	9.072(–5)
8.8	0.6801	6.167(–5)	0.2997	2.206(–3)	1.129(–4)	3.123(–3)	1.978(–6)	8.729(–3)	1.281(–5)	1.566(–5)	5.439(–6)	1.250(–4)	5.914(–5)	7.413(–5)	9.070(–5)
8.9	0.6802	6.147(–5)	0.2997	2.205(–3)	1.118(–4)	3.124(–3)	1.979(–6)	8.730(–3)	1.272(–5)	1.565(–5)	5.443(–6)	1.250(–4)	5.912(–5)	7.411(–5)	9.072(–5)
9.0	0.6803	6.114(–5)	0.2996	2.202(–3)	1.113(–4)	3.131(–3)	1.978(–6)	8.727(–3)	1.270(–5)	1.561(–5)	5.446(–6)	1.249(–4)	5.924(–5)	7.409(–5)	9.074(–5)
9.1	0.6800	6.082(–5)	0.2998	2.199(–3)	1.113(–4)	3.139(–3)	1.974(–6)	8.721(–3)	1.250(–5)	1.559(–5)	5.460(–6)	1.249(–4)	5.926(–5)	7.405(–5)	9.079(–5)
9.3	0.6792	6.051(–5)	0.3007	2.189(–3)	1.108(–4)	3.175(–3)	1.969(–6)	8.695(–3)	1.241(–5)	1.551(–5)	5.499(–6)	1.243(–4)	5.987(–5)	7.391(–5)	9.093(–5)
9.5	0.6802	5.995(–5)	0.2997	2.206(–3)	1.128(–4)	3.130(–3)	1.971(–6)	8.721(–3)	1.198(–5)	1.563(–5)	5.477(–6)	1.250(–4)	5.914(–5)	7.397(–5)	9.087(–5)
10.0	0.6793	5.892(–5)	0.3006	2.194(–3)	1.127(–4)	3.168(–3)	1.951(–6)	8.695(–3)	1.160(–5)	1.553(–5)	5.534(–6)	1.244(–4)	5.975(–5)	7.377(–5)	9.108(–5)
10.5	0.6801	5.775(–5)	0.2997	2.199(–3)	1.140(–4)	3.157(–3)	1.946(–6)	8.699(–3)	1.121(–5)	1.555(–5)	5.535(–6)	1.246(–4)	5.958(–5)	7.372(–5)	9.112(–5)

Table 5. Envelope mass fraction of selected species at the end of the 2DUP.

$M_{\rm ini}$	^{1}H	^{3}He	^{4}He	^{12}C	^{13}C	^{14}N	^{15}N	^{16}O	^{17}O	^{18}O	^{21}Ne	^{22}Ne	^{23}Na	^{25}Mg	^{26}Mg
	$Z = 0.00001$														
7.0	0.6436	2.557(–5)	0.3563	2.136(–6)	3.418(–8)	3.404(–6)	1.710(–9)	3.065(–6)	4.919(–8)	5.313(–9)	9.508(–9)	3.322(–8)	6.188(–8)	2.070(–8)	5.153(–8)
7.5	0.6383	2.327(–5)	0.3617	1.730(–5)	3.402(–8)	3.437(–6)	1.694(–9)	3.079(–6)	4.615(–8)	2.026(–8)	9.573(–9)	4.010(–8)	6.316(–8)	2.017(–8)	5.189(–8)
7.7	0.6374	2.260(–5)	0.3626	2.083(–5)	3.393(–8)	3.456(–6)	1.688(–9)	3.081(–6)	4.524(–8)	2.190(–8)	9.502(–9)	4.299(–8)	6.501(–8)	2.001(–8)	5.180(–8)
8.0	0.6358	2.145(–5)	0.3642	3.754(–5)	3.475(–8)	3.458(–6)	1.688(–9)	3.189(–6)	4.363(–8)	2.750(–8)	9.516(–9)	5.410(–8)	6.455(–8)	1.977(–8)	5.204(–8)
8.5	0.6320	1.987(–5)	0.3679	1.001(–4)	3.401(–8)	3.484(–6)	1.677(–9)	4.091(–6)	4.126(–8)	3.092(–8)	9.478(–9)	7.688(–8)	6.589(–8)	1.933(–8)	5.198(–8)
9.0	0.6290	1.857(–5)	0.3706	3.109(–4)	3.380(–8)	3.486(–6)	1.674(–9)	1.025(–5)	3.926(–8)	3.448(–8)	9.386(–9)	1.163(–7)	6.612(–8)	1.885(–8)	5.119(–8)
9.5	0.7431	2.100(–5)	0.2568	5.272(–7)	3.664(–8)	3.030(–6)	1.988(–9)	3.444(–6)	4.495(–8)	3.788(–9)	1.128(–8)	3.703(–8)	8.163(–8)	2.181(–8)	5.717(–8)
10.0	0.7381	2.013(–5)	0.2619	5.246(–7)	3.661(–8)	3.042(–6)	1.969(–9)	3.435(–6)	4.331(–8)	3.762(–9)	1.118(–8)	3.687(–8)	7.191(–8)	2.171(–8)	5.670(–8)
10.5	0.7382	1.938(–5)	0.2618	5.255(–7)	3.679(–8)	3.031(–6)	1.989(–9)	3.448(–6)	4.205(–8)	3.763(–9)	1.102(–8)	3.699(–8)	6.641(–8)	2.160(–8)	5.738(–8)
11.0	0.7414	1.863(–5)	0.2586	5.208(–7)	3.703(–8)	3.027(–6)	1.970(–9)	3.460(–6)	4.118(–8)	3.731(–9)	1.148(–8)	3.697(–8)	6.798(–8)	2.150(–8)	5.835(–8)
11.5	0.7342	1.797(–5)	0.2657	5.199(–7)	3.679(–8)	3.064(–6)	2.001(–9)	3.420(–6)	3.950(–8)	3.707(–9)	1.048(–8)	3.664(–8)	6.532(–8)	2.104(–8)	5.624(–8)
12.0	0.7299	1.720(–5)	0.2701	5.168(–7)	3.680(–8)	3.085(–6)	2.001(–9)	3.403(–6)	3.788(–8)	3.673(–9)	1.002(–8)	3.643(–8)	6.093(–8)	2.083(–8)	5.593(–8)
	$Z = 0.0001$														
7.0	0.6423	4.461(–5)	0.3575	8.947(–6)	3.911(–7)	2.769(–5)	1.616(–8)	3.606(–5)	4.790(–7)	7.802(–8)	5.846(–8)	4.139(–7)	7.970(–7)	2.551(–7)	4.625(–7)
7.2	0.6414	4.362(–5)	0.3584	1.007(–5)	3.903(–7)	2.793(–5)	1.613(–8)	3.582(–5)	4.696(–7)	9.444(–8)	5.755(–8)	4.136(–7)	7.799(–7)	2.521(–7)	4.648(–7)
7.5	0.6374	4.184(–5)	0.3624	2.675(–5)	3.894(–7)	2.800(–5)	1.608(–8)	3.569(–5)	4.519(–7)	2.288(–7)	5.763(–8)	5.140(–7)	7.426(–7)	2.506(–7)	4.614(–7)
8.0	0.6344	3.972(–5)	0.3654	6.402(–5)	3.892(–7)	2.811(–5)	1.608(–8)	3.576(–5)	4.293(–7)	2.917(–7)	5.708(–8)	7.381(–7)	6.974(–7)	2.466(–7)	4.622(–7)
8.5	0.6319	3.786(–5)	0.3678	1.744(–4)	4.500(–7)	2.829(–5)	1.607(–8)	3.769(–5)	4.081(–7)	3.214(–7)	5.658(–8)	1.019(–6)	6.812(–7)	2.431(–7)	4.629(–7)
9.0	0.6290	3.629(–5)	0.3706	1.707(–4)	3.882(–7)	2.856(–5)	1.606(–8)	3.691(–5)	3.854(–7)	3.479(–7)	5.591(–8)	1.088(–6)	6.771(–7)	2.396(–7)	4.631(–7)
9.5	0.7413	4.182(–5)	0.2586	6.844(–6)	4.258(–7)	2.274(–5)	1.875(–8)	4.091(–5)	4.429(–7)	4.951(–8)	6.690(–8)	4.647(–7)	7.152(–7)	2.792(–7)	5.444(–7)
10.0	0.7421	4.078(–5)	0.2577	6.845(–6)	4.278(–7)	2.275(–5)	1.889(–8)	4.091(–5)	4.243(–7)	4.943(–8)	6.615(–8)	4.650(–7)	7.152(–7)	2.787(–7)	5.452(–7)
10.5	0.7373	3.992(–5)	0.2625	6.824(–6)	4.286(–7)	2.309(–5)	1.899(–8)	4.058(–5)	3.959(–7)	4.919(–8)	6.348(–8)	4.637(–7)	7.809(–7)	2.742(–7)	5.405(–7)
11.0	0.7408	3.891(–5)	0.2591	6.804(–6)	4.299(–7)	2.332(–5)	1.906(–8)	4.039(–5)	3.545(–7)	4.893(–8)	6.364(–8)	4.624(–7)	7.755(–7)	2.720(–7)	5.471(–7)
11.5	0.7359	3.817(–5)	0.2640	6.786(–6)	4.300(–7)	2.333(–5)	1.914(–8)	4.039(–5)	3.656(–7)	4.874(–8)	6.303(–8)	4.615(–7)	8.334(–7)	2.699(–7)	5.399(–7)
12.0	0.7285	3.726(–5)	0.2714	6.739(–6)	4.325(–7)	2.328(–5)	1.896(–8)	4.050(–5)	3.632(–7)	4.842(–8)	6.347(–8)	4.620(–7)	9.024(–7)	2.687(–7)	5.268(–7)
	$Z = 0.001$														
7.5	0.6377	5.023(–5)	0.3612	8.886(–5)	4.422(–6)	2.394(–4)	8.239(–8)	3.839(–4)	2.467(–6)	1.909(–6)	3.408(–7)	5.367(–6)	8.959(–6)	3.055(–6)	4.915(–6)
7.7	0.6359	4.915(–5)	0.3630	9.257(–5)	4.416(–6)	2.414(–4)	8.201(–8)	3.817(–4)	2.423(–6)	2.181(–6)	3.499(–7)	5.667(–6)	9.064(–6)	3.036(–6)	4.925(–6)
8.0	0.6344	4.796(–5)	0.3645	1.134(–4)	4.420(–6)	2.412(–4)	8.192(–8)	3.807(–4)	2.354(–6)	2.820(–6)	3.468(–7)	7.115(–6)	9.224(–6)	3.025(–6)	4.916(–6)
8.5	0.6322	4.617(–5)	0.3667	1.829(–4)	4.409(–6)	2.441(–4)	8.145(–8)	3.776(–4)	2.239(–6)	3.090(–6)	3.705(–7)	9.309(–6)	9.360(–6)	2.985(–6)	4.936(–6)
9.0	0.6274	4.423(–5)	0.3710	5.819(–4)	4.557(–6)	2.447(–4)	8.084(–8)	3.977(–4)	2.139(–6)	3.488(–6)	3.662(–7)	1.355(–5)	9.692(–6)	2.957(–6)	4.931(–6)
9.5	0.7394	5.100(–5)	0.2596	8.665(–5)	4.900(–6)	1.835(–4)	9.118(–8)	4.362(–4)	2.343(–6)	6.236(–7)	4.623(–7)	5.633(–6)	3.750(–6)	3.467(–6)	4.784(–6)
10.0	0.7412	5.001(–5)	0.2577	8.656(–5)	4.916(–6)	1.838(–4)	9.113(–8)	4.359(–4)	2.337(–6)	6.223(–7)	4.491(–7)	5.631(–6)	3.713(–6)	3.467(–6)	4.788(–6)

Table 5. continued.

$M_{\rm ini}$	^{1}H	^{3}He	^{4}He	^{12}C	^{13}C	^{14}N	^{15}N	^{16}O	^{17}O	^{18}O	^{21}Ne	^{22}Ne	^{23}Na	^{25}Mg	^{26}Mg
10.5	0.7376	4.924(–5)	0.2614	8.720(–5)	4.968(–6)	1.830(–4)	9.159(–8)	4.362(–4)	2.111(–6)	6.260(–7)	4.363(–7)	5.679(–6)	3.831(–6)	3.458(–6)	4.792(–6)
11.0	0.7289	4.803(–5)	0.2700	8.664(–5)	4.978(–6)	1.917(–4)	9.128(–8)	4.272(–4)	1.769(–6)	6.203(–7)	4.423(–7)	5.634(–6)	4.224(–6)	3.376(–6)	4.863(–6)
11.5	0.7302	4.737(–5)	0.2687	8.680(–5)	4.997(–6)	1.896(–4)	9.130(–8)	4.294(–4)	1.819(–6)	6.209(–7)	4.184(–7)	5.651(–6)	4.207(–6)	3.393(–6)	4.846(–6)
12.0	0.7292	4.642(–5)	0.2697	8.596(–5)	4.968(–6)	1.883(–4)	9.041(–8)	4.318(–4)	2.033(–6)	6.144(–7)	3.786(–7)	5.610(–6)	4.352(–6)	3.416(–6)	4.818(–6)
	$Z = 0.004$														
8.1	0.6340	5.214(–5)	0.3620	3.619(–4)	1.881(–5)	9.105(–4)	3.262(–7)	1.543(–3)	4.309(–6)	8.928(–6)	1.170(–6)	2.526(–5)	2.022(–5)	1.262(–5)	2.024(–5)
8.3	0.6332	5.141(–5)	0.3627	3.689(–4)	1.884(–5)	9.107(–4)	3.254(–7)	1.542(–3)	4.279(–6)	9.637(–6)	1.160(–6)	2.734(–5)	2.046(–5)	1.259(–5)	2.025(–5)
8.5	0.6315	5.060(–5)	0.3644	3.717(–4)	1.882(–5)	9.186(–4)	3.243(–7)	1.533(–3)	4.211(–6)	1.053(–5)	1.165(–6)	2.834(–5)	2.065(–5)	1.253(–5)	2.032(–5)
8.0	0.6352	5.256(–5)	0.3607	3.532(–4)	1.881(–5)	9.104(–4)	3.267(–7)	1.547(–3)	4.392(–6)	6.897(–6)	1.177(–6)	2.248(–5)	2.008(–5)	1.265(–5)	2.021(–5)
9.0	0.6278	4.888(–5)	0.3679	6.099(–4)	1.954(–5)	9.162(–4)	3.213(–7)	1.529(–3)	3.993(–6)	1.258(–5)	1.157(–6)	4.890(–5)	2.112(–5)	1.242(–5)	2.041(–5)
9.5	0.6250	4.750(–5)	0.3706	5.714(–4)	1.880(–5)	9.271(–4)	3.195(–7)	1.514(–3)	3.832(–6)	1.280(–5)	1.173(–6)	5.154(–5)	2.152(–5)	1.231(–5)	2.051(–5)
10.0	0.7304	5.427(–5)	0.2656	3.863(–4)	2.094(–5)	6.870(–4)	3.538(–7)	1.748(–3)	4.264(–6)	2.756(–6)	1.356(–6)	2.430(–5)	1.255(–5)	1.432(–5)	1.867(–5)
10.5	0.7253	5.168(–5)	0.2706	3.826(–4)	2.228(–5)	7.078(–4)	3.369(–7)	1.728(–3)	3.740(–6)	2.741(–6)	1.514(–6)	2.421(–5)	1.264(–5)	1.409(–5)	1.890(–5)
11.0	0.7268	5.192(–5)	0.2691	3.880(–4)	2.212(–5)	6.942(–4)	3.437(–7)	1.737(–3)	3.776(–6)	2.769(–6)	1.467(–6)	2.432(–5)	1.256(–5)	1.417(–5)	1.883(–5)
11.5	0.7230	5.076(–5)	0.2729	3.856(–4)	2.230(–5)	7.055(–4)	3.397(–7)	1.727(–3)	3.582(–6)	2.750(–6)	1.553(–6)	2.421(–5)	1.274(–5)	1.405(–5)	1.894(–5)
12.0	0.7148	4.884(–5)	0.2811	3.792(–4)	2.278(–5)	7.470(–4)	3.275(–7)	1.689(–3)	2.602(–6)	2.705(–6)	1.744(–6)	2.385(–5)	1.322(–5)	1.370(–5)	1.930(–5)
13.0	0.7140	4.961(–5)	0.2819	3.854(–4)	2.167(–5)	7.525(–4)	3.507(–7)	1.675(–3)	2.792(–6)	2.728(–6)	1.730(–6)	2.372(–5)	1.348(–5)	1.360(–5)	1.940(–5)
	$Z = 0.008$														
8.0	0.6382	5.451(–5)	0.3538	7.254(–4)	3.858(–5)	1.750(–3)	6.742(–7)	3.137(–3)	7.139(–6)	5.913(–6)	2.899(–6)	4.370(–5)	3.237(–5)	2.616(–5)	3.977(–5)
8.3	0.6352	5.353(–5)	0.3567	7.304(–4)	3.855(–5)	1.763(–3)	6.727(–7)	3.118(–3)	6.082(–6)	1.307(–5)	2.797(–6)	4.615(–5)	3.260(–5)	2.599(–5)	3.993(–5)
8.5	0.6342	5.280(–5)	0.3577	7.334(–4)	3.855(–5)	1.765(–3)	6.689(–7)	3.114(–3)	5.990(–6)	1.536(–5)	2.727(–6)	4.911(–5)	3.282(–5)	2.594(–5)	3.998(–5)
8.6	0.6322	5.216(–5)	0.3597	7.333(–4)	3.878(–5)	1.783(–3)	6.643(–7)	3.095(–3)	5.838(–6)	1.669(–5)	2.734(–6)	5.136(–5)	3.309(–5)	2.581(–5)	4.011(–5)
8.8	0.6294	5.173(–5)	0.3625	7.388(–4)	3.814(–5)	1.799(–3)	6.688(–7)	3.074(–3)	5.726(–6)	1.821(–5)	2.706(–6)	5.339(–5)	3.357(–5)	2.564(–5)	4.028(–5)
9.0	0.6288	5.053(–5)	0.3631	7.353(–4)	3.841(–5)	1.806(–3)	6.602(–7)	3.071(–3)	6.504(–6)	1.913(–5)	2.670(–6)	5.410(–5)	3.419(–5)	2.560(–5)	4.032(–5)
9.5	0.6246	4.899(–5)	0.3673	7.395(–4)	3.837(–5)	1.836(–3)	6.538(–7)	3.038(–3)	6.221(–6)	2.085(–5)	2.607(–6)	5.895(–5)	3.499(–5)	2.533(–5)	4.059(–5)
10.0	0.6189	4.702(–5)	0.3725	1.195(–3)	3.946(–5)	1.819(–3)	6.329(–7)	3.050(–3)	6.045(–6)	2.559(–5)	2.432(–6)	1.077(–4)	3.591(–5)	2.512(–5)	4.076(–5)
10.5	0.7181	5.314(–5)	0.2738	7.909(–4)	4.412(–5)	1.358(–3)	6.919(–7)	3.489(–3)	6.631(–6)	5.635(–6)	2.407(–6)	4.912(–5)	2.457(–5)	2.906(–5)	3.690(–5)
11.0	0.7116	4.904(–5)	0.2803	7.528(–4)	4.447(–5)	1.479(–3)	6.420(–7)	3.402(–3)	6.457(–6)	5.371(–6)	2.641(–6)	4.735(–5)	2.638(–5)	2.848(–5)	3.746(–5)
11.5	0.7045	4.691(–5)	0.2874	7.347(–4)	4.455(–5)	1.555(–3)	6.207(–7)	3.340(–3)	6.149(–6)	5.238(–6)	2.884(–6)	4.642(–5)	2.732(–5)	2.796(–5)	3.801(–5)
12.0	0.6995	4.541(–5)	0.2924	7.237(–4)	4.509(–5)	1.604(–3)	6.084(–7)	3.299(–3)	5.750(–6)	5.159(–6)	3.055(–6)	4.572(–5)	2.807(–5)	2.760(–5)	3.837(–5)
13.0	0.6930	3.999(–5)	0.2989	6.313(–4)	3.604(–5)	1.781(–3)	5.793(–7)	3.230(–3)	6.294(–6)	4.405(–6)	3.281(–6)	4.385(–5)	3.009(–5)	2.706(–5)	3.893(–5)
	$Z = 0.02$														
8.8	0.6022	4.910(–5)	0.3777	1.812(–3)	1.001(–4)	4.406(–3)	1.602(–6)	7.796(–3)	1.427(–5)	3.013(–5)	7.131(–6)	1.128(–4)	7.721(–5)	6.739(–5)	9.719(–5)
9.0	0.6002	4.841(–5)	0.3796	1.815(–3)	1.001(–4)	4.425(–3)	1.593(–6)	7.762(–3)	1.407(–5)	4.224(–5)	7.114(–6)	1.275(–4)	7.794(–5)	6.712(–5)	9.742(–5)
9.5	0.5970	4.695(–5)	0.3828	1.819(–3)	1.004(–4)	4.480(–3)	1.576(–6)	7.705(–3)	1.349(–5)	4.845(–5)	7.022(–6)	1.399(–4)	7.920(–5)	6.664(–5)	9.784(–5)
10.0	0.5929	4.565(–5)	0.3868	1.938(–3)	1.002(–4)	4.519(–3)	1.554(–6)	7.637(–3)	1.297(–5)	5.965(–5)	6.939(–6)	1.918(–4)	8.057(–5)	6.607(–5)	9.834(–5)
10.5	0.5912	4.467(–5)	0.3880	2.404(–3)	1.004(–4)	4.511(–3)	1.541(–6)	7.632(–3)	1.257(–5)	6.631(–5)	6.808(–6)	2.597(–4)	8.151(–5)	6.573(–5)	9.868(–5)
11.0	0.6828	5.085(–5)	0.2970	1.996(–3)	1.119(–4)	3.396(–3)	1.700(–6)	8.699(–3)	1.397(–5)	1.416(–5)	5.479(–6)	1.219(–4)	6.250(–5)	7.378(–5)	9.100(–5)
11.3	0.6818	5.026(–5)	0.2980	1.990(–3)	1.122(–4)	3.430(–3)	1.688(–6)	8.668(–3)	1.375(–5)	1.410(–5)	5.525(–6)	1.213(–4)	6.305(–5)	7.361(–5)	9.118(–5)
11.5	0.6815	4.997(–5)	0.2984	1.988(–3)	1.124(–4)	3.443(–3)	1.685(–6)	8.654(–3)	1.356(–5)	1.409(–5)	5.548(–6)	1.211(–4)	6.327(–5)	7.353(–5)	9.127(–5)
12.0	0.6756	4.853(–5)	0.3042	1.960(–3)	1.128(–4)	3.580(–3)	1.649(–6)	8.537(–3)	1.274(–5)	1.387(–5)	5.772(–6)	1.196(–4)	6.481(–5)	7.282(–5)	9.200(–5)
	$Z = 0.04$														
9.0	0.5587	4.793(–5)	0.4011	3.765(–3)	2.006(–4)	8.313(–3)	3.343(–6)	1.595(–2)	2.863(–5)	6.827(–5)	1.258(–5)	2.339(–4)	1.510(–4)	1.411(–4)	1.882(–4)
9.2	0.5594	4.789(–5)	0.4004	3.802(–3)	2.022(–4)	8.155(–3)	3.351(–6)	1.605(–2)	3.317(–5)	8.556(–5)	1.249(–5)	2.739(–4)	1.499(–4)	1.413(–4)	1.879(–4)
9.5	0.5551	4.660(–5)	0.4047	3.760(–3)	2.006(–4)	8.398(–3)	3.300(–6)	1.582(–2)	2.783(–5)	9.767(–5)	1.268(–5)	3.075(–4)	1.540(–4)	1.403(–4)	1.889(–4)
10.0	0.5526	4.564(–5)	0.4055	4.679(–3)	2.010(–4)	8.347(–3)	3.274(–6)	1.638(–2)	2.618(–5)	1.094(–4)	1.272(–5)	5.209(–4)	1.547(–4)	1.395(–4)	1.903(–4)
10.5	0.5496	4.468(–5)	0.4083	5.078(–3)	2.160(–4)	8.375(–3)	3.238(–6)	1.600(–2)	2.562(–5)	1.259(–4)	1.280(–5)	6.546(–4)	1.572(–4)	1.423(–4)	1.981(–4)
11.0	0.6315	5.062(–5)	0.3282	4.159(–3)	2.238(–4)	6.345(–3)	3.564(–6)	1.768(–2)	2.792(–5)	2.931(–5)	1.032(–5)	2.450(–4)	1.238(–4)	1.495(–4)	1.799(–4)
11.5	0.6318	5.014(–5)	0.3280	4.164(–3)	2.255(–4)	6.345(–3)	3.550(–6)	1.768(–2)	2.696(–5)	2.932(–5)	1.034(–5)	2.451(–4)	1.237(–4)	1.494(–4)	1.801(–4)
12.0	0.6311	4.947(–5)	0.3286	4.157(–3)	2.274(–4)	6.395(–3)	3.523(–6)	1.763(–2)	2.666(–5)	2.925(–5)	1.038(–5)	2.437(–4)	1.252(–4)	1.492(–4)	1.803(–4)
13.0	0.6291	4.829(–5)	0.3306	4.136(–3)	2.291(–4)	6.513(–3)	3.475(–6)	1.752(–2)	2.494(–5)	2.903(–5)	1.052(–5)	2.420(–4)	1.270(–4)	1.487(–4)	1.809(–4)
	overshooting $Z = 0.0001$														
5.0	0.6488	6.742(–5)	0.3510	7.024(–6)	4.059(–7)	2.488(–5)	1.816(–8)	3.832(–5)	5.350(–7)	5.133(–8)	6.694(–8)	4.605(–7)	1.058(–6)	2.653(–7)	4.639(–7)
5.5	0.6418	6.004(–5)	0.3581	9.903(–6)	4.031(–7)	2.563(–5)	1.764(–8)	3.762(–5)	5.139(–7)	7.941(–8)	6.662(–8)	4.502(–7)	1.022(–6)	2.602(–7)	4.597(–7)
5.7	0.6338	5.578(–5)	0.3660	1.843(–5)	3.967(–7)	2.642(–5)	1.710(–8)	3.694(–5)	4.917(–7)	1.705(–7)	6.330(–8)	4.645(–7)	1.043(–6)	2.542(–7)	4.561(–7)
6.0	0.6348	5.395(–5)	0.3650	3.887(–5)	4.117(–7)	2.657(–5)	1.704(–8)	3.709(–5)	4.879(–7)	2.758(–7)	6.459(–8)	5.839(–7)	9.548(–7)	2.548(–7)	4.562(–7)
7.0	0.6198	4.571(–5)	0.3792	7.841(–4)	6.643(–7)	2.767(–5)	1.659(–8)	1.226(–4)	4.302(–7)	3.561(–7)	6.177(–8)	1.342(–6)	8.574(–7)	2.435(–7)	4.494(–7)
7.5	0.6187	4.326(–5)	0.3781	2.363(–3)	4.483(–5)	1.002(–4)	6.255(–8)	5.863(–4)	1.038(–6)	1.474(–6)	6.793(–8)	7.293(–6)	8.014(–7)	4.751(–7)	4.904(–7)
8.0	0.7419	4.945(–5)	0.2580	7.289(–6)	4.383(–7)	2.095(–5)	1.948(–8)	4.231(–5)	4.848(–7)	5.329(–8)	7.069(–8)	4.951(–7)	6.307(–7)	2.878(–7)	5.391(–7)
9.0	0.7417	4.594(–5)	0.2582	7.282(–6)	4.463(–7)	2.113(–5)	1.973(–8)	4.214(–5)	4.447(–7)	5.297(–8)	6.933(–8)	4.928(–7)	6.668(–7)	2.834(–7)	5.417(–7)
10.0	0.7390	4.283(–5)	0.2608	7.172(–6)	4.447(–7)	2.174(–5)	1.972(–8)	4.163(–5)	4.034(–7)	5.197(–8)	6.799(–8)	4.881(–7)	7.505(–7)	2.767(–7)	5.415(–7)
	overshooting $Z = 0.02$														
7.0	0.5967	5.872(–5)	0.3832	1.906(–3)	1.002(–4)	4.367(–3)	1.749(–6)	7.712(–3)	1.474(–5)	3.827(–5)	7.285(–6)	1.170(–4)	7.636(–5)	6.798(–5)	9.685(–5)
7.5	0.5935	5.587(–5)	0.3863	1.914(–3)	1.001(–4)	4.398(–3)	1.729(–6)	7.662(–3)	1.377(–5)	5.275(–5)	7.253(–6)	1.455(–4)	7.750(–5)	6.741(–5)	9.736(–5)
8.0	0.5909	5.378(–5)	0.3886	2.212(–3)	1.012(–4)	4.356(–3)	1.722(–6)	7.633(–3)	1.318(–5)	6.424(–5)	7.191(–6)	2.521(–4)	7.850(–5)	6.694(–5)	9.782(–5)
8.5	0.5908	5.205(–5)	0.3873	3.177(–3)	1.249(–4)	4.343(–3)	1.706(–6)	7.916(–3)	1.259(–5)	6.796(–5)	7.161(–6)	3.294(–4)	7.912(–5)	6.888(–5)	1.028(–4)
8.8	0.5845	5.043(–5)	0.3926	4.038(–3)	1.216(–4)	4.345(–3)	1.706(–6)	7.985(–3)	1.212(–5)	5.288(–5)	7.197(–6)	4.350(–4)	8.087(–5)	6.869(–5)	1.035(–4)
8.9	0.6577	5.657(–5)	0.3221	2.064(–3)	1.115(–4)	3.559(–3)	1.816(–6)	8.421(–3)	1.342(–5)	1.466(–5)	6.056(–6)	1.191(–4)	6.564(–5)	7.198(–5)	9.244(–5)
9.0	0.6769	5.784(–5)	0.3029	2.113(–3)	1.125(–4)	3.303(–3)	1.853(–6)	8.648(–3)	1.381(–5)	1.504(–5)	5.583(–6)	1.223(–4)	6.194(–5)	7.367(–5)	9.098(–5)
9.1	0.6768	5.751(–5)	0.3031	2.109(–3)	1.126(–4)	3.313(–3)	1.849(–6)	8.641(–3)	1.356(–5)	1.501(–5)	5.591(–6)	1.223(–4)	6.201(–5)	7.363(–5)	9.101(–5)
9.3	0.6775	5.732(–5)	0.3023	2.104(–3)	1.123(–4)	3.321(–3)	1.845(–6)	8.639(–3)	1.349(–5)	1.497(–5)	5.572(–6)	1.220(–4)	6.224(–5)	7.366(–5)	9.105(–5)
9.5	0.6790	5.684(–5)	0.3009	2.123(–3)	1.145(–4)	3.266(–3)	1.847(–6)	8.675(–3)	1.307(–5)	1.510(–5)	5.532(–6)	1.229(–4)	6.138(–5)	7.378(–5)	9.097(–5)
10.0	0.6783	5.581(–5)	0.3015	2.110(–3)	1.145(–4)	3.302(–3)	1.825(–6)	8.651(–3)	1.268(–5)	1.499(–5)	5.580(–6)	1.223(–4)	6.195(–5)	7.360(–5)	9.116(–5)
10.5	0.6793	5.472(–5)	0.3006	2.114(–3)	1.156(–4)	3.292(–3)	1.822(–6)	8.657(–3)	1.230(–5)	1.500(–5)	5.578(–6)	1.225(–4)	6.181(–5)	7.356(–5)	9.120(–5)